

**COMPUTATIONAL STUDIES ON THE INTERACTION OF
DIRECT DYE, PHTHALATE, PESTICIDE FROM
WASTEWATER WITH COPPEROXIDE NANOPARTICLES**



By

Kashmala Nadeem

326116

Supervisor

Dr. Uzma Habib

MS Computational Science and Engineering

School of Interdisciplinary Engineering and Sciences (SINES)

National University of Sciences and Technology (NUST)

Islamabad, Pakistan

2024

COMPUTATIONAL STUDIES ON THE INTERACTION OF
DIRECT DYE, PHYTHALE, PESTICIDE FROM WASTEWATER
WITH COPPEROXIDE NANOPARTICLES



By

Kashmala Nadeem

326116

Supervisor

Dr. Uzma Habib

A thesis submitted in partial fulfillment of the requirement for the
degree of Masters of Science

in

Computational Science and Engineering

School of Interdisciplinary Engineering and Sciences (SINES)

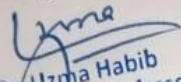
National University of Sciences and Technology (NUST)

Islamabad, Pakistan

2024


THESIS ACCEPTANCE CERTIFICATE

Certified that final copy of MS/MPhil thesis written by Ms. **Kashmala Nadeem** Registration No. **00000326116** of **SINES** has been vetted by undersigned, found complete in all aspects as per NUST Statutes/Regulations, is free of plagiarism, errors, and mistakes and is accepted as partial fulfillment for award of MS/MPhil degree. It is further certified that necessary amendments as pointed out by GEC members of the scholar have also been incorporated in the said thesis.

Signature with stamp: 
Dr. Uzma Habib
Associate Professor
SINES - NUST, Sector H-12
Islamabad

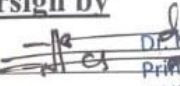
Name of Supervisor: Dr. Uzma Habib

Date: 12-01-24

Signature of HoD with stamp: 
Dr. Fouzia Malik
HoD Sciences
Professor
SINES - NUST, Sector H 12
Islamabad

Date: 12-01-2024

Countersign by

Signature (Dean/Principal): 
Dr. Hammad M. Cheema
Principal & Dean
SINES - NUST, Sector H-12
Islamabad

Date: 15/01/2024

Declaration

I, Kashmala Nadeem declare that this thesis titled “COMPUTATIONAL STUDIES ON THE REMOVAL OF DIRECT DYE, PHYTHALE, PESTICIDE FROM WASTEWATER BY ADSORPTION ON THE SURFACE OF COPPEROXIDE NANOPARTICLES” and the work presented in it are my own and has been generated by me as a result of my own original research.

I confirm that:

1. This work was done wholly or mainly while in candidature for a Master of Science degree at NUST

2. Where any part of this thesis has previously been submitted for a degree or any other qualification at NUST or any other institution, this has been clearly stated

3. Where I have consulted the published work of others, this is always clearly attributed

4. Where I have quoted from the work of others, the source is always given. With the exception of such quotations, this thesis is entirely my own work

5. I have acknowledged all main sources of help

6. Where the thesis is based on work done by myself jointly with others, I have made clear exactly what was done by others and what I have contributed myself

Kashmala Nadeem,

Spring2020-MS CSE-00000326116

This thesis is dedicated to my beloved *Father Nadeem Ahmad* and my *Mother Miss Munawar Sultana* I would pay special regards to my mother who continuously helped me emotionally and morally throughout my life. Without her support I am unable to achieve my goals

Acknowledgment

First of all, my heartily gratitude is to Almighty Allah for giving me the valor to complete this research project. Secondly, I am extremely grateful and indebted to my research supervisor, associate professor Dr. Uzma Habib for her expert, valuable, and sincere guidance, and encouragement during this research. I owe my deepest gratitude to my GEC members, Dr.ishrat jabeen associate professor at school of interdisciplinary engineering and sciences (SINES), NUST and Dr. Mudassir Iqbal associate Professor at school of natural sciences (SNS), NUST, for their boundless support and guidance. Last, but not the least, I would like to say a very special thanks to my friends and family, especially my affectionate parents and my siblings for their love, care, and support during the course of this project.

Kashmala Nadeem

Table of Contents

Chapter 1 Introduction	1
1.1 Copper oxide	1
1.2 Properties of Copper Oxide:	1
1.2.1 Crystal structure of CuO:.....	2
1.2.2 Electrical conductivity of CuO:	2
1.2.3 Thermal conductivity of CuO:	2
1.2.4 Stability of CuO:	2
1.3 Nanoparticles	2
1.3.1 Copper Oxide Nanoparticles:	3
1.4 Water pollution	5
1.5 Components of Wastewater	5
1.5.1 Dyes.....	5
1.5.2 Pesticides	9
1.5.3 Phthalates	11
1.6 Waste Water Treatment	13
1.6.1 Methods of removal.....	13
1.7 Adsorption.....	15
1.7.1 Chemisorption:.....	16
1.7.2 Physiosorption:	16
1.7.3 Exothermic:	16
1.7.4 Endothermic:.....	17
1.8 Factors affecting Adsorption.....	17
1.8.1 Effect of initial concentration of adsorbate	17
1.8.2 Effect of pH	19
1.8.3 Effect of adsorbent particle size	19
1.8.4 Effect of solution temperature.	20
Chapter 2 Literature Review	21
2.1 Background	22
2.2 Copper Oxide Nanoparticles.....	23
2.3 Water pollutants	24
2.3.1 Direct Yellow Dye	24

2.3.2 Bifenthrin	27
2.3.3 Dioctyl Phthalate.....	29
2.4 Metal Oxide	31
2.4.1 Titanium Oxide.....	31
2.4.2 Zinc oxide Nanoparticles.....	34
2.5 Problem Statement:.....	35
2.6 Objectives	36
Chapter 3 Methodology	37
3.1 Computational Software:	38
3.2 Amsterdam Density Functional (ADF) Software	38
3.3 Density Functional Theory (DFT) Studies:	39
3.3 Taxonomy for function	40
3.3.1 GGA Functional	41
3.3.2 Basis Set	41
3.3.3 Double Zeta Basis set	42
Chapter 4 Results and Discussions	44
4.1 Geometry optimization and electronic structure.....	44
4.1.1 Copper Oxide Nanoparticle.....	45
4.1.2 Bifenthrin (pesticide)	46
4.1.3 Dioctyl Phthalate.....	51
4.1.4 Direct Yellow Dye	55
Chapter 5 Discussion:	63
Chapter 6 Conclusion.....	66
6.1 Future Perspectives	66
References.....	68

List of Figures

Figure 1.1 (a) Basic Dye Structure (Methylene Blue) (b) computational structure.....	7
Figure 1.2 (a) Acidic dye Structure (Orange dye) (b) computational structure.....	8
Figure 1.3 Direct yellow dye (direct yellow 24).....	8
Figure 1.4 Disperse dye structure (disperse yellow 26).....	9
Figure 1.5 Azo dye Structure	9
Figure 1.6 adsorption process [57].....	15
Figure 2.1 Percentage of different pollutants in water [80]	22
Figure 2.2 pollutants and their side effects[121].....	36
Figure 3.1 Methodology flow chart for computational modeling.....	37
Figure 4.1 represents CuO nanoparticle (red ball shows oxygen atom whereas golden ball shows copper atom)	45
Figure 4.2 (a) The geometry optimized structure of Bifenthrin (light blue balls: carbon, Green ball: fluorine, red balls: oxygen, small light blue balls: hydrogen, pea green balls: Chlorine) CuO attraction at (b) central position (c) terminal position	46
Figure 4.3 (a&b) Bifenthrin after CuO NPs possible attraction surfaces showing the preferred place of adsorption between dye and adsorbent.	47
Figure 4.4 (a&b) The atomic bond distances of CuO NPs adsorption on bifenthrin (Golden Ball: Copper, Red Ball: Oxygen, Light Blue Ball: Carbon, Dark Green Ball: Fluorine, Pea Green Ball: Chlorine & Small blue Ball: Hydrogen).	48
Figure 4.5 Binding energies for CuO Adsorbed at (a) Terminal position of bifenthrin, (b) Central position of Bifenthrin.....	50
Figure 4.6 represents geometry optimized structure of Dioctyl phthalate (light blue: carbon, red balls: oxygen, small light blue balls: hydrogen) b) and c) Dioctyl phthalate have oxygen(s) as a possible site for attraction or adsorption with CuO NPs.....	52
Figure 4.7 (a&b) shows the HOMO-LUMO image of dye adsorption for dioctyl phthalate	52
Figure 4.8 (a&b) The atomic bond distances of CuO NPs adsorption on dioctyl phthalate (Golden Ball: Copper, Red Ball: Oxygen, Light Blue Ball: Carbon, & Small blue Ball: Hydrogen).	53
Figure 4.9 (a&b) Binding energies of CuO adsorbed at two different ester group oxygen sites of Dioctylphthalate.....	54
Figure 4.10 (a) The geometry optimized structure of direct yellow dye (light blue balls: carbon, Dark blue balls: nitrogen, red balls: oxygen, small light blue balls: hydrogen, green balls:sodium, yellow balls: Sulphur).....	56
Figure 4.11 (a,b&c) shows the HOMO-LUMO energy gaps.....	57

Figure 4.12 (a,b&c) The atomic bond distances of CuO NPs adsorption on direct yellow (Red Ball: Oxygen, Light Blue Ball: Carbon, Dark Green Ball: Fluorine, Navy Blue Ball: Nitrogen, Yellow Ball: Sulphur, Green Ball: Sodium and Small White Ball: Hydrogen)..... 58

Figure 4.13 shows binding energy of direct yellow dye from the point of a) attachment of CuO with nitrogen of azo group where sulphonic acid group is present b) shows attached of CuO NP from sulphonic group site c) represents attachment of CuO NP with the azo group..... 60

List of Tables

Table 1.1 Properties of copper oxide	1
Table 1.2 Biological method [50] [51, 52].....	14
Table 1.3 Chemical methods [49, 52, 53]	14
Table 1.4 Physical methods [50, 54, 55].....	15
Table 2.1 Adsorption capacity of TiO ₂ against different adsorbates.....	33
Table 2.2 Adsorption capacity of ZnO ₂ against different adsorbates.....	35
Table 3.1 Parameters for the DFT studies of CuO NP and the waste water pollutants.	42
Table 4.1 the binding energy, enthalpy, entropy of CuO NPs and (BF,DOP and DYD) before adsorption. The values obtained because of most stable geometries.....	45
Table 4.2 Atomic bond distance and Mulliken's charges on atoms on dye (bifenthrin) and CuO NPs.....	49
Table 4.3 represents the optimized energy value and adsorption energy values of CuO and bifenthrin before and after adsorption on two different angles.....	50
Table 4.4 The atomic bond distances and Mulliken's charges for the atoms of dioctyl phthalate dye and CuO NPs.....	53
Table 4.5 represents the optimized energy value and adsorption energy values of CuO and dioctylphthalate before and after adsorption on two different angles.....	54
Table 4.6 (a,b&c) The atomic bond distances and Mulliken's charges for the atoms of direct yellow dye and CuO NPs.....	59
Table 4.7 represents the optimized energy value and adsorption energy values of CuO and DYD before and after adsorption on three different sites.	61
Table 4.8 showing adsorption energy and binding energy values of waste water components with different angles.....	Error! Bookmark not defined.
Table 4.9 calculated HOMO LOMO and energy gap values of waste water components with different angles.....	Error! Bookmark not defined.

Abstract

Dyes, pesticides, phthalates have wide applications in various industries like paint, textile, fertilizers, plastic and paper industries. They are released as waste materials by these industries during cleaning process and have detrimental impacts on aquatic environment. Now a days heterogenous catalysis and adsorption studies have been gaining much popularity worldwide due to its versatility. Reported data shows that many adsorbents were used to remove these components like activated carbon, zeolites some metal oxide like TiO_2 , ZnO , however they are expensive and highly toxic. So present research focused on the nanoparticle which is cheap, less toxic and remove maximum number of pollutants from waste water. Heterogenous adsorption mechanism of three components namely, bifenthrin, dioctyl phthalate and direct yellow dye with Copper Oxide (CuO) was probed to determine interaction prosperity on basis of computational kinetics. In this work Density Functional Theory (DFT) at the energy level of GGA/PW91 basis set double zeta (DZ) was conducted to evaluate the interaction behavior of Copper oxide nanoparticle with Direct yellow dye, Bifenthrin, and dioctylphthalate. Calculated electronic (E_{HOMO} , E_{LUMO}), kinetic (E_{ad}), and thermodynamic parameters (ΔG , ΔH , and ΔS) based on quantum chemical DFT approach revealed highest interaction of direct yellow dye-24 with Copper oxide (CuO) nanoparticle which is -3.2758eV, -2.5783 for dioctyl phthalate, -0.3767 for bifenthrin. This research would have tremendous impact in the area of water purification and desalination using Copperoxide (CuO) nanoparticles. We can enhance the removal of a maximum number of wastewater pollutants by employing copper oxide nanoparticles for water purification. This approach is advantageous due to its cost-effectiveness, less-toxic nature, and high adsorption efficiency.

Chapter 1 Introduction

1.1 Copper oxide

The 25th most common element in the Earth crust is copper. Oxygen and copper combine to form the substance known as copper oxide. Depending on the oxidation state of copper, it can appear in a variety of ways, including copper (I) oxide (Cu₂O) and copper (II) oxide (CuO). Copper (Cu) has an oxidation state of +2, which indicates the loss of two electrons, whereas oxygen (O) has an oxidation state of -2, which indicates the gain of two electrons, in the case of CuO (copper(II) oxide) [1].

1.2 Properties of Copper Oxide:

The characteristics of copper oxide (CuO) are presented in Table 1.1:

Table 1.1 Properties of copper oxide

Property	Description	Merits	Ref.
Structure/Morphology	Monoclinic	Space group: C2/c	[1]
Electrical Conductivity (EC)	Low EC: $\approx 1.2\text{eV}$	EC can be enhanced at nanoscale.	[2]
Thermal Conductivity (TC)	Highly resistant to strong TC potential	Suitable for thermal insulation.	[3]
Stability	Highly stable for normal solid state	Strong practical applications and long-term performance.	[4]

1.2.1 Crystal structure of CuO:

CuO has a monoclinic structure in the C2/c space group. It contains copper ions (Cu^{2+}) arranged in a square planar coordination and oxygen ions (O^{2-}) forming a face-centered cubic lattice. The bonding between copper and oxygen involves covalent and ionic interactions [1].

1.2.2 Electrical conductivity of CuO:

CuO is an electrical insulator and possesses a bandgap of around 1.2 eV. It exhibits low electrical conductivity due to the absence of freely moving charge carriers. However, the conductivity of CuO can be enhanced through doping or by reducing its size to the nanoscale [2].

1.2.3 Thermal conductivity of CuO:

CuO has poor thermal conductivity compared to metals and other oxide materials. The low thermal conductivity of CuO makes it suitable for applications where thermal insulation is desired [3].

1.2.4 Stability of CuO:

CuO is generally stable under normal conditions. However, its stability can be affected by the factors such as temperature, atmosphere, and exposure to reducing or oxidizing agents.[3] Understanding the stability of CuO is essential for its practical applications and long-term performance.

1.3 Nanoparticles

Nanoparticles are the particles that have sizes ranging from 1 to 100 nanometers (nm). At this scale, the particles exhibit unique physical, chemical, and biological properties that differ from their bulk counterparts.[4]

Nanoparticles can be composed of various materials, including metals, metal oxides, semiconductors, polymers, and biological substances. They can be synthesized through a variety of methods, such as chemical reduction, precipitation, sol-gel processes, vapor deposition techniques, and green methods.

1.3.1 Copper Oxide Nanoparticles:

Copper is present everywhere in the environment, naturally. In the Earth's crust, there is a concentration of approximately 146 parts per million (ppm), which is equivalent to around 60 grams per metric ton.[5] Copper oxide nanoparticles, which consist of small particles of copper and oxygen, have attracted considerable attention for their potential in adsorption processes.

1.3.1.1 Properties of Copper Oxide Nanoparticles

Some of the properties of copper oxide nanoparticles are;

1.3.1.1.1 Antimicrobial activity:

Copper oxide nanoparticles exhibit strong antimicrobial properties, effectively inhibiting the growth of bacteria, viruses, and fungi in water [6]. They can disrupt the cell membranes of microorganisms and generate reactive oxygen species (ROS), leading to microbial inactivation.

1.3.1.1.2 Surface area:

Copper oxide nanoparticles have a high surface area-to-volume ratio due to their small size. This increased surface area enhances their reactivity and provides more active sites for interaction with contaminants, facilitating the removal of pollutants from water [4].

1.3.1.1.3 Adsorption capability:

Copper oxide nanoparticles can adsorb and bind to a variety of contaminants present in water, including heavy metals, organic pollutants, and dyes. This adsorption capacity helps in the removal of these pollutants and contributes to the purification of water [4].

1.3.1.1.4 Catalytic activity:

Copper oxide nanoparticles possess catalytic activity, enabling them to participate in oxidation and reduction reactions [7]. This property is useful for the degradation of organic pollutants through processes like advanced oxidation, where contaminants are effectively broken down into harmless byproducts.

1.3.1.1.5 Regenerability:

Copper oxide nanoparticles can be regenerated and reused in water treatment processes. By removing the accumulated contaminants or by refreshing the surface, the nanoparticles can maintain their efficacy over multiple cycles, contributing to cost-effectiveness [8].

1.3.1.1.6 Stability and Durability:

Copper oxide nanoparticles are generally stable and resistant to oxidation, ensuring their long-term performance in water treatment applications. They can withstand varying pH levels and temperature conditions without significant degradation.[9]

1.3.1.1.7 Concentration Requirement:

Copper oxide nanoparticles can exhibit effective antimicrobial and contaminant removal properties even at low concentrations. This property reduces the amount of nanoparticles required for water treatment, making it a cost-effective option.[10]

1.3.1.1.8 Environmental Compatibility:

Copper oxide is considered less toxic to humans and the environment compared to certain chemical disinfectants or heavy metals. The use of copper oxide nanoparticles in water treatment offers an environmentally friendly alternative while ensuring effective disinfection and pollutant removal [8].

1.3.1.1.9 Surface Sensitivity:

The high surface area of nanoparticles makes them highly sensitive to surface-related phenomena, such as adsorption, desorption, and surface reactions. This sensitivity enables their use in sensors and analytical devices [11].

1.4 Water pollution

Now a day's water pollution is a major concern. It has been a current global challenge and environmental issue [12-14].The water quantity, quality and availability is a major concern in many areas of the world because of anthropogenic activities such as industrialization, domestic usage, agricultural activities, population expansion. The poor quality of water affects more than 1.2 billion people and roughly costs the lives of 15 million children every year [15]. Due to water pollution 2.2 million deaths occur globally[12]

1.5 Components of Wastewater

There are various components of wastewater which includes pathogens, dyes, pesticides, fertilizers, heavy metals, phthalates, pharmaceuticals products, radioactive substances etc. My research will cover the following four components of wastewater:

- Dyes
- Pesticides
- Phthalates

1.5.1 Dyes

The process of adding colors to materials such as paper, fabrics and other items is known as dyeing. Humans have used dyes for more than 1000 years in a variety of ways [10]. Back to 3500 BC dyes were made from naturally available materials made such as plants, insects etc. and

were known as natural dyes but the disadvantage of natural dyes was it restricted the range of colors as well as its muted tone which are faded while washing or exposing to sunlight [16, 17].

Synthetic dyes were discovered in 1876 and their production on a large scale is increasing because of its high demand. A large variety of synthetic dyes were invented by WH Perkins spotting various brilliant colorfast tones for numerous uses [16]. So the retention of natural dyes has been solved by the invention of synthetic dyes, which leads to another problem of water pollution. The dye effluents are released in water without any proper treatment. So, the presence of dye effluents in water becomes a threat to living organisms due to its toxic nature [18]. If we resume the natural dye usage it was found that it is as harmful as utilizing synthetic dyes alone [19]. Mordants, a chemical, usually an inorganic oxide, that reacts with a dye or stain and fixes it in a material, it serve as binding agents that assist in the bonding of natural dyes to materials. However, it is important to note that mordants can be highly toxic and pose greater risks compared to synthetic dyes [12].

Synthetic dyes are stable as well as complex structures due to the presence of chromophores (color giving compound) and auxochromes (water soluble bonding compound) [16, 20, 21]. This quality complicates the degradation of dyes using simple methods. So why the dyes are created this way? The reason might be that the colors of dyed materials do not fade easily [22]. They are made as complex molecules (organic) so that they can resist while degraded upon contact with detergents, water or any other agents which are used in washing [23]. Dyes molecules have strong resistance even when exposed to strong light, heat sources, oxidizing agents. [24, 25].

1.5.1.1 Types of Dyes

Based on molecular structures there are many types of dyes, classified based on their application and solubility. Basic dyes, acidic dyes, direct dyes are the examples of soluble dyes. Azo dyes, disperse dyes, sulphur dyes and vat dyes are the examples of insoluble dyes.

1.5.1.1.1 Basic Dyes

This type of dyes is also known as cationic dyes because they have a hydroxyl group (OH) and in the aqueous medium these dyes can be dissociated into charged ions. Also, basic dyes are bright in colors. They are toxic (water-soluble) but have less intensity of toxicity as compared to acidic dyes. They are used in the dyeing of fabric and leather [26, 27]. For example, Methylene Blue

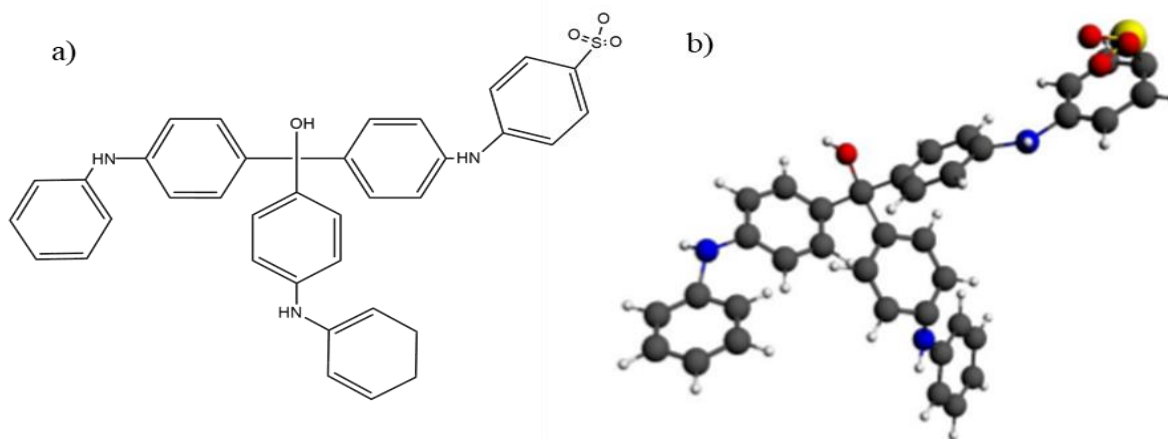


Figure 1.1 (a) Basic Dye Structure (Methylene Blue)

(b) computational structure

1.5.1.1.2 Acidic Dyes.

They are also known as anionic dyes and in aqueous medium they can be dissociated into (negatively) charge ions They are more reactive as compared to basic dyes due to the presence of reactive azo-group (-N=N-), Sulphur (-S=S-), or oxygen (-O=O-) [28-30]. The example of acidic dyes is orange dye.

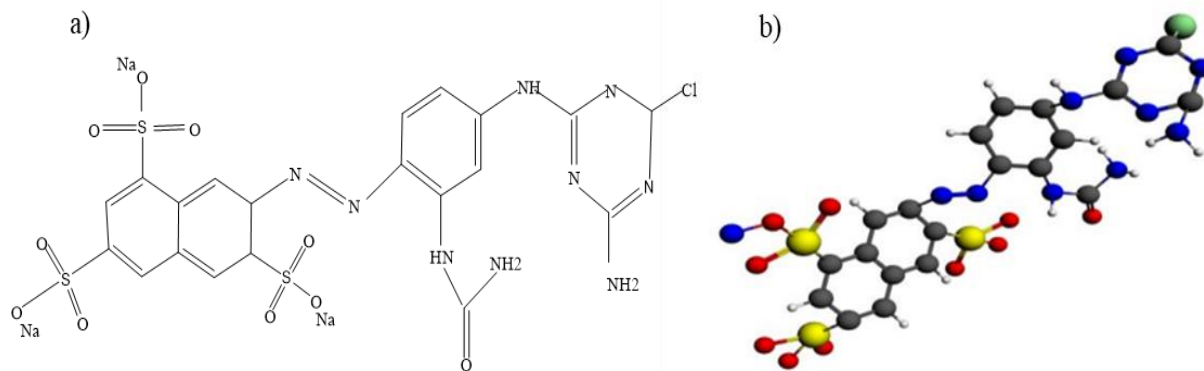


Figure 1.2 (a) Acidic dye Structure (Orange dye)

(b) computational structure

1.5.1.1.3 Direct dyes

Direct dyes, usually referred to as substantive dyes, are a class of water-soluble substances that have a built-in affinity for fibers. They, especially benzidine compounds, can be immediately absorbed by the fibers. These dyes produce brilliant and vivid color results while being generally affordable and easy to use. Our study is also based on direct dyes. One of the example of Direct dyes is Direct Yellow 24.[31]

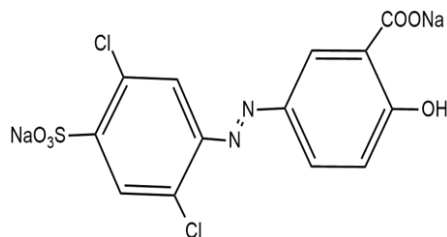


Figure 1.3 Direct yellow dye (direct yellow 24)

1.5.1.1.4 Disperse Dyes

The term "disperse dye" describes organic coloring agents that don't have ionizing groups, have a poor water solubility, and are excellent for coloring hydrophobic fibers. It must be applied

in the form of an aqueous dispersion and is insoluble in water [32]. An example of disperse dyes is Disperse yellow 26.

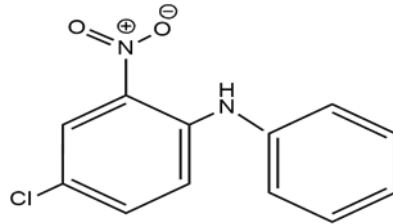


Figure 1.4 Disperse dye structure (disperse yellow 26)

1.5.1.1.5 Vat dyes

Vat dyes are a large class of water-insoluble dyes that are frequently used to color cellulosic fibers. They include indigo and anthraquinonoid derivatives. The dye is applied to the fiber in a soluble, reduced form and subsequently oxidized in the fiber to its original insoluble state.[33]

1.5.1.1.6 Azo dyes

Organic substances with the functional group $RN=NR'$, in which R and R' are typically aryl and substituted aryl groups, are known as azo dyes. They are a family of commercially significant azo compounds, or substances that contain the C-N=N-C connection. Azo dyes are artificial dyes that are not found in nature [34-37].

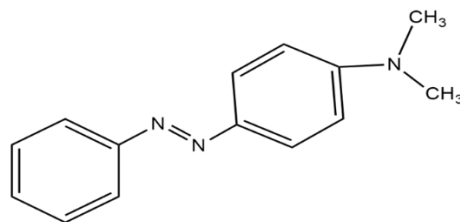


Figure 1.5 Azo dye Structure

1.5.2 Pesticides

Pesticides are chemical substances or mixtures employed for the purpose of managing, repelling, or eradicating pests, encompassing insects, weeds, fungi, and rodents. They find

widespread usage in agriculture, public health, and various industries to safeguard crops, prevent disease transmission, and preserve product quality [38]. Some types of pesticides are presented below.

1.5.2.1 Herbicides:

In order to control or get rid of unwanted weeds and plants, herbicides are used. They can either be non-selective, harming a wide variety of plants, or selective, focusing on particular plant kinds[39]. Examples of some common herbicides are 2,4-D, atrazine, and glyphosate.

1.5.2.2 Fungicides:

To prevent or treat fungal diseases in trees, crops, and other plants, fungicides are used. They can be divided into three categories according to how they work: protectant fungicides, contact fungicides, and systemic fungicides.[40]. Captan, thiophanate-methyl and azoxystrobin, are the few examples.

1.5.2.3 Rodenticides:

Rodenticides are the compounds used to manage rodent populations, including mice and rats. These pesticides are designed to attract and poison rodents [41]. Rodenticides like warfarin, bromadiolone, and diphacinone are frequently used.

1.5.2.4 Insecticides:

These pesticides are designed specifically to target and control insects. They can be further classified into different groups based on their mode of action, such as organophosphates, carbamates, pyrethroids, neonicotinoids, and botanical insecticides [42]. The target of my research is bifenthrin insecticide.

1.5.2.4.1 Bifenthrin:

The class of currently used pesticides are synthetic pesticides produced for the control of pests in residential areas and agriculture. As compared to other traditional pesticides for example organochlorine and organophosphate, the synthetic pyrethroid show very effective insecticidal activity to a high range of pests and relatively low acute toxicity to birds and mammals.[40] That is why pyrethroid insecticides, over the past decades have been increasingly popular, approx. 25 percent of the global insecticides market [41].

Because of its widespread application, the residues of bifenthrin insecticide has been frequently detected in residential area, environmental media, biota (flora and fauna regions), thus posing potential hazards to the health of wildlife and human beings. Bifenthrin in particular is the main source of pesticide toxicity in water and demonstrates strong acute fatal toxicity to aquatic species. Bifenthrin can also have sublethal toxic effects on a variety of non-target creatures (human beings), including oxidative damage, neurobehavioral toxicity, developmental toxicity, immunological toxicity, and effects the endocrine system [41]

1.5.3 Phthalates

Phthalates, which are extensively manufactured, form the largest category of synthetic chemicals in terms of production volume. These compounds serve as plasticizers in various polymer goods. However, there is growing apprehension regarding their potential harm to both human health and ecosystems [43]. Consequently, regulations have been implemented to prohibit the use of phthalates in children's toys and related items as they are recognized for their ability to disrupt the endocrine system.

Phthalates are the chemical compounds that consist of diesters of 1,2-benzenedicarboxylic acid (phthalic acid), featuring a benzene ring with two ester functional groups [44]. Their solubility in water is generally low, and it decreases as the length of the side chain (the alcohol moiety) or the molecular weight (MW) of the compound increases. Consequently, phthalates with shorter alkyl groups (lower molecular weights) like DMP and DBP exhibit greater water solubility compared to the long-chained phthalates. The volatility of phthalates at standard temperature is generally low, especially for long-chain phthalates such as DEHP and BBP [45].

The uses of different phthalates predominantly depend on their molecular weight (MW). Higher MW phthalates like DEHP, DiNP, and DiDP are utilized in the production of construction materials and various PVC products, including clothing items (such as footwear and raincoats), flooring and wall coverings, food packaging, children's products (toys, grip bumpers), and medical devices. On the other hand, manufacturers employ low MW phthalates such as di-methyl phthalate (DMP), di-ethyl phthalate (DEP), and DBP as solvents in personal care products (such as perfumes, lotions, and cosmetics), insecticides, lacquers, and coatings, including those that provide controlled release in certain pharmaceuticals. They are also utilized in PVC applications [46].

1.5.3.1 Dioctyl phthalate

Dioctyl phthalate (DOP) is an ester compound derived from phthalic acid. Its molecular structure includes a benzene ring with two ester functional groups, each connected to an octyl alcohol chain composed of eight carbon atoms. DOP is commonly utilized as a plasticizer, serving to enhance the flexibility, durability, and workability of polymers [47]. It finds extensive application in industries such as vinyl flooring manufacturing, synthetic leather production, wire and cable coatings, automotive component fabrication, and the creation of medical devices. Nevertheless, similar to other phthalates, concerns exist regarding the potential adverse impacts of

DOP on both human health and the environment, specifically its ability to disrupt the endocrine system [48].

1.6 Waste Water Treatment

There are various methods which are used for the removal of these waste water components (specifically direct yellow dye, bifenthrin, dioctyl phthalate) from water such as biological, chemical and physical methods. These methods are discussed below with in a table[49].

1.6.1 Methods of removal

These pollutants (dyes, pesticides, phthalates) can be removed from water by using three methods chemicals, physical, biological methods some of these methods are presented with its merits and demerits in a table below:

Table 1.2 Biological method [50] [51, 52]

S.No	Methods	Descriptions	Merits	Demerits
1	Pure and Mixed Culture.	Mixture of bacteria, algae, fungi along with differed chemicals used to remove pollutants	Reusable, easy to operate	Release colorless by-products.
2	Enzyme Degradation.	The extracted enzymes are used to degrade dyes	Eco friendly process, cheap.	Unreliable amount of enzyme production
3	Algae Degradation.	pollutants are consumed b algae for self-growth	Cheap, nontoxic, more efficient.	Makes system unstable

Table 1.3 Chemical methods [49, 52, 53]

S.No	Methods	Descriptions	Merits	Demerits
1	Electrochemical Destruction.	Non stable anodes are used to eat up enzymes	No chemical consume, no sludge production.	High cost, less effective pollutants removal method
2	Ozonation	pollutants are eliminated by ozone produced from oxygen	Straightforward method, short reaction time	Makes system unstable, produce toxic biproducts
3	Ultraviolet irradiation	Use UV light to decompose pollutants	No sludge production,	High cost, energy depletion

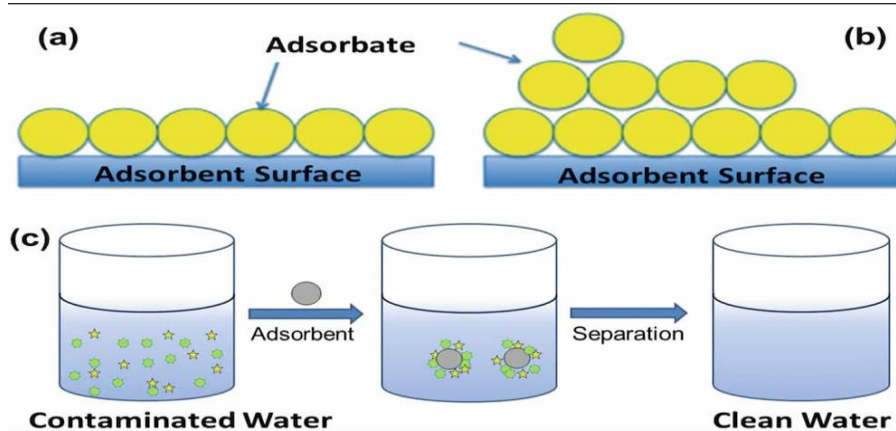
Table 1.4 Physical methods [50, 54, 55]

S.No	Methods	Descriptions	Merits	Demerits
1	Nanofiltration ultra violet filtration	The waste water undergo filtration using a fine pored membrane that isolated pollutants particles from purified water.	Remove any type of wastewater component.	High cost, high energy consumption, short life span
2	Irradiation	Radiation is used to remove waste water molecules	Effective at laboratory scale	Huge amount of dissolve oxygen required
3	Adsorption	High adsorption capacity materials are used to adsorb pollutants	Excellent method of removal for variety of wastewater components.	Adsorbents can be costly

Among all the above mentioned techniques adsorption is found to be best and most effective technique for the removal of waste materials from water such as dyes, pesticides, phthalate etc

1.7 Adsorption

Adsorption can be defined as a phenomenon of mass transfer, wherein elements accumulate at the boundary between two alike or dissimilar phases. This interaction occurs across various phases such as gas-liquid, gas-solid, liquid-liquid, and liquid-solid interfaces [52, 56].

**Figure 1.6** adsorption process [57]

Adsorption can be classified into these main types:

1.7.1 Chemisorption:

Chemisorption refers to the formation of strong covalent bonds between the adsorbent and adsorbate. It involves a chemical reaction between the two [56]. The process of chemisorption is influenced by the temperature, an increase in temperature leads to increased chemisorption. This is because higher temperatures provide the necessary energy for the formation of stronger chemical bonds between the adsorbent and adsorbate.

1.7.2 Physisorption:

Physical adsorption, also known as physisorption, involves weak van der Waals forces between the adsorbent and adsorbate. It is characterized by relatively weaker interactions compared to chemisorption. The relationship between physisorption and temperature is inverse. As increase in temperature leads to decrease in physical adsorption. This is because higher temperatures provide greater thermal energy, which can overcome the weak van der Waals forces between the adsorbent and adsorbate, resulting in reduced adsorption.[58, 59].

1.7.3 Exothermic:

In exothermic adsorption, the efficiency of the adsorption process decreases with an increase in temperature. This can be attributed to the weakening of adsorptive forces between the adsorbate and the active sites of the adsorbent as the temperature rises. Consequently, the dye removal efficiency is reduced [60]. Exothermic adsorption is commonly employed to regulate the diffusion process, as the mobility of dye ions increases with the addition of heat to the system [61].

1.7.4 Endothermic:

On the other hand, in endothermic adsorption, the efficiency of the adsorption process increases with a rise in temperature. This is due to a higher availability of active sites resulting from the activation of the adsorbent surface at higher temperatures [62]. The increase in adsorption capacity by raising the temperature can be attributed to the enhanced mobility of the larger dye ions [63].

1.8 Factors affecting Adsorption.

The efficiency of liquid phase adsorption and, consequently, the proper operation of the water treatment process, depends on a number of factors. The properties of the used adsorbent, the type of the pollutant (in this study, the phthalate, pesticide, dyes,), and the chemical composition of the pollutant all have an impact on the sorption effectiveness.[52] These physical and chemical variables include the interaction between the adsorbent and the adsorbate, the surface chemistry and pore structure of the adsorbent, particle size, the inherent properties of the adsorbent, the presence of other ions in the aqueous solution, temperature, pressure, pH levels, and the contact time. In addition, it is important to take into account the characteristics of the substance being adsorbed, including its size, polarity, molecular weight, and molecular structure [64]. The most influencing factors (particle size, and temperature, initial dye concentration, adsorbent volume, aqueous solution pH) are discussed below.

1.8.1 Effect of initial concentration of adsorbate

The concentration of adsorbate at the beginning of the process plays a crucial role in affecting the adsorption process. This influence is seen in its impact on the number of binding sites available on the adsorbent surface, subsequently influencing the effectiveness of adsorbate [64].

In water treatment setups, the effectiveness (E) of removing the adsorbate and the equilibrium capacity (q) for maximum adsorbate binding are intimately connected to the initial adsorbate concentration [65].

$$E(\%) = \frac{C_i - C_f}{C_i} \cdot 100$$

$$q = \frac{(C_i - C_f) \cdot V}{m}$$

where E represents efficiency, q stands for the equilibrium dye binding capacity in milligrams per gram (mg/g), C_i represents the initial concentration in milligrams per liter (mg/L), C_e represents the final adsorbate concentration in mg/L, m represents the amount of adsorbent in grams (g), and V represents the volume of the aqueous solution in liters (L).

If the concentration of the solution increases and the amount of bound material follows a similar trend, then at low initial solution concentration the surface area of the adsorbent and the number of adsorption binding sites are high, allowing contaminant ions or molecules (in our case, dye molecules) to bind easily to the adsorbent surface. Conversely, higher initial solution concentrations curtail the total available adsorption sites, potentially resulting in a reduction in the percentage of contaminant removal. The elevation at higher initial concentrations could be attributed to intensified driving forces [66, 67].

During low concentrations, the ratio of active sites to adsorbate molecules tends to be high, enabling swift interaction of all molecules with the adsorbent and near-instantaneous removal from the solution [68].

1.8.2 Effect of pH

As evidenced by multiple studies, the pH of the adsorbate solution emerges as a pivotal factor across a wide array of adsorption processes. This parameter wields influence over both the adsorbent's capacity and the process's overall efficiency.[69]

The pH exerts its impact through several mechanisms: it shapes the solution chemistry of contaminants, modulates the activity of functional groups within the adsorbent, influences the competitive interactions with coexisting ions in the solution, and governs the surface charge of the adsorbent. Moreover, the pH of the aqueous medium possesses the capability to mold the properties of the adsorbent itself, the intricacies of the adsorption mechanism, and the dissociation patterns of dye molecules. Notably, the pH can even induce alterations in the chemical structure of both the adsorbent and the adsorbate. An intriguing consequence of pH variation is the transformation of the surface charge and ionization degree of the adsorbed ion [70-73].

1.8.3 Effect of adsorbent particle size

While often overlooked in biosorption investigations, particle size can significantly influence heterogeneous chemical reactions and adsorption processes [74]. Smaller particle dimensions yield a heightened specific surface area, a crucial parameter for sorption phenomena. Specific surface area (SSA) denotes the total surface area of a solid material per unit of mass and holds significance for sorption processes. The SSA is contingent upon particle size, material structure, and porosity [75], commonly quantified in m^2/g .

The correlation between adsorption capacity and particle size hinges on two key factors [76, 77]:

- The chemical attributes of the dye molecule, encompassing its ionic charge and hydrolysis potential.

- The inherent characteristics of the adsorbent, encompassing crystallinity, porosity, and the rigidity of its polymeric chains.

In the realm of static batch adsorption methods, smaller particle sizes tend to foster augmented adsorption capacity and efficiency, primarily attributable to the greater availability of active binding sites.

1.8.4 Effect of solution temperature.

Temperature constitutes a noteworthy physico-chemical parameter that exerts a significant influence, orchestrating shifts in the treatment process from endothermic to exothermic reactions, or vice versa [78]. Additionally, its impact on adsorption is robust, capable of inducing either augmentation or reduction in adsorption quantities [79].

The sway of temperature on sorption efficiency manifests diversely, contingent upon the adsorbent and the pollutant in question. Generally, it amplifies the bio sorption of impurities, boosting surface activity and kinetic energy of the adsorbate, albeit with the potential to impair the physical structure of the biosorbent.

- With ascending temperatures, the pace of chemical reactions accelerates. Consequently, if the sorption process adheres to chemisorption principles ($\Delta H_{\text{chemisorption}} = -200 \text{ kJ/mol}$), heightened temperatures yield enhanced sorption efficiency, ultimately attaining equilibrium.
- Conversely, when dealing with physical adsorption ($\Delta H_{\text{physisorption}} \approx -20 \text{ kJ/mol}$), elevated temperatures exert an adverse effect on adsorption. Moreover, temperature possesses the capacity to elicit chemical modifications within the adsorbent, thereby influencing its adsorption sites and activity.

Chapter 2 Literature Review

This literature review chapter explains the unique potential of copper oxide nanoparticles for wastewater remediation, with a focus on their physical adsorption method application. As the demand for pure water increases on a global scale, it becomes imperative to address the contamination of water sources, necessitating the development of innovative techniques for efficient pollutant removal. Due to their remarkable physicochemical properties and their capacity for adsorption-based processes, copper oxide nanoparticles have garnered considerable interest in this context. This chapter evaluates the properties of copper oxide nanoparticles, elucidates their underlying adsorption mechanisms, and investigates their efficacy in removing a variety of effluent contaminants. By elucidating the intricate relationship between nanoparticle properties and adsorption performance, this study contributes to the expanding understanding of advanced materials designed for sustainable and efficient environmental solutions.

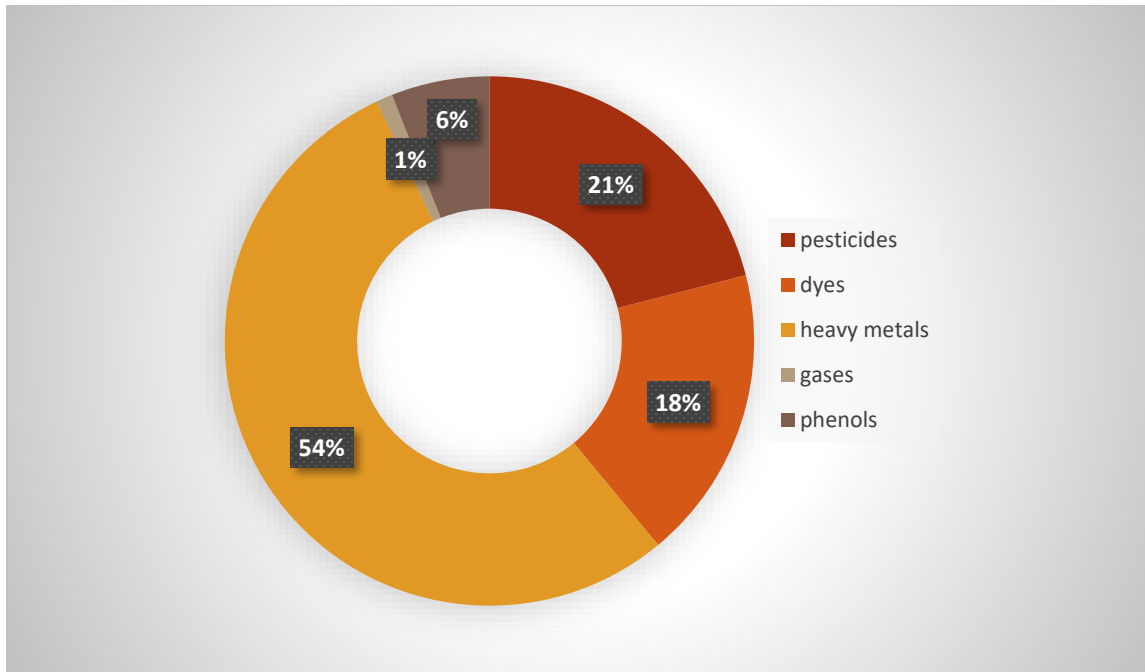


Figure 2.1 Percentage of different pollutants in water [80]

2.1 Background

In recent years, there has been a significant surge in research focusing on the elimination of waste from wastewater through the adsorption method. Of all the contaminants present in water, some components are particularly hazardous and possess a significant risk to the environment. Among various wastewater removal techniques, adsorption has emerged as an exceptionally effective and economical approach.

Industries release a lot of byproducts as waste, and these byproducts can be efficiently separated by utilizing adsorbents such as metal oxide nanoparticles, metal surfaces, and activated carbon. The adsorption capacity of these byproduct components depends on the surface area and temperature of the adsorbent material. Both theoretical and experimental studies have demonstrated that these waste water components such as (direct yellow dye, bifenthrin, dioctyl phthalate) can be effectively removed using cost-effective and readily available new adsorbents.

Therefore, the search for efficient and affordable adsorbents derived from readily available materials has become increasingly important in recent years for the successful removal of pollutants like (dyes, pesticides, phthalates) from wastewater.

2.2 Copper Oxide Nanoparticles

Copper oxide nanoparticles (CuO NPs) have been extensively studied as highly effective adsorbent materials, owing to their small size, large surface area, abundance in starting materials for synthesis, cost-effective production processing, and non-toxic properties. This literature review chapter focuses on the adsorption of pollutants by CuO NPs, aiming to consolidate recent research findings, identify knowledge gaps, and propose potential areas for future investigations [13].

Conventional chemical processes such as microwave heating and precipitation are commonly employed for synthesizing CuO NPs. Notably, the highest reported adsorption capacity of CuO NPs was observed for fluoride, with a remarkable removal capacity of over three times its own weight from the aqueous phase (3152 mg/g) [13]. The most suitable kinetic and isotherm models for adsorption using CuO NPs were found to be the pseudo-second order model ($R^2 > 0.99$) and Langmuir model ($R^2 > 0.99$), respectively, for dyes and heavy metals [49]. Thermodynamic analysis demonstrated that the adsorption process of CuO NPs was mainly spontaneous and endothermic.

An important aspect is that CuO NPs can be efficiently reused for up to five cycles, with a recovery rate of >80% of pollutants in most cases [13]. However, future work should explore mechanistic investigations using statistical physics, competitive adsorption studies, and column experiments. Given the negative eco-toxicological impact of CuO NPs, it is crucial to exercise caution and ensure their proper removal or recovery from wastewater before any environmental

release [49]. Despite this, it can be inferred that CuO NPs exhibit great potential as an effective adsorbent for mitigating various pollutants in the aqueous environment.

2.3 Water pollutants

This research is focusing on the removal of below mentioned pollutants from wastewater

- 1 Direct Yellow Dye
- 2 Bifenthrin (pesticide)
- 3 Dioctyl phthalate (plasticizer)

2.3.1 Direct Yellow Dye

Through literature some of the physical methods for the removal of DYD from wastewater are discussed below

G. Ravathi in 2011 [81] studied the successful removal of DYD from aqueous solutions using *Jatropha Curcus L. tree leaves activated carbon (JCTC)*. This research examines various factors, including different concentrations of the dye, pH levels, and contact time. A high adsorption rate of 87.05% for 1g of JCTC, with optimal conditions at pH 7.8 and a temperature of $27\pm 1^\circ\text{C}$ was observed. The removal efficiency increases from 22.65 to 39.31 mg/g as the dye concentration rises from 30 to 60 ppm, but the percentage of dye adsorbed decreases from 75.50% to 65.52% under the same conditions. Equilibrium is reached in 20 minutes, and the adsorption process is favorable ($RL \sim 1$). The equilibrium sorption capacity is 0.361, allowing treatment of 261.89 L/g. Column experiments reveal linear relationships with bed depth and contact time, following first-order kinetics. The data fits various kinetic models, and SEM and FT-IR analyses confirm physical adsorption mechanisms rather than chemical reactions [81].

In 2019 the study by Liang Gui wang [82] inquired into the adsorption of Direct Yellow dye from aqueous solutions using *bamboo charcoals* activated with various agents, including *orthophosphoric acid*, *nitric acid*, *potassium hydroxide*, and *zinc chloride*. In batch adsorption experiments, it was determined that the optimal sorption conditions, including an initial dye concentration of 24.62 mg/L, a pH of 1.0, a contact time of 21 hours, and a temperature of 298 K, yielded different maximum adsorption capacities. The bamboo charcoal activated with orthophosphoric acid exhibited the highest capacity at 2.401 mg/g, while the lowest capacity of 1.705 mg/g was observed for the bamboo charcoal activated with potassium hydroxide[82].

To understand the kinetics of the adsorption process, various models were considered, and the Avrami kinetic model was found to provide the best fit to the experimental data, surpassing other models like Elovich, pseudo-first-order, pseudo-second-order, and intra-particle diffusion. When examining the equilibrium data, the Langmuir, Freundlich, Jovanovic, Khan, and Koble-Corrigan isotherm models were applied. Among these, the Koble-Corrigan model demonstrated the best fit, with three-parameter models showing superior fitting compared to two-parameter models[82].

Thermodynamic analysis unveiled that the adsorption process was spontaneous and endothermic, indicating a physical nature of adsorption. Notably, the bamboo charcoal activated with orthophosphoric acid outperformed the other activated charcoals in terms of Direct Yellow dye removal. This research highlights the potential of orthophosphoric acid-activated bamboo charcoal as an effective adsorbent for the removal of this dye from aqueous solutions[82].

In another research, *Monika Wawrzkiwicz* 2019 [83] investigates the adsorption capabilities of a *silica-titanium mixed oxide with an 80 wt.% SiO₂ and 20 wt.% TiO₂ composition (ST₂₀)* concerning C.I. Direct Yellow (DY) dye. This study reveals that (Silica-titanium 20) has an

experimental adsorption capacity for DY of 104.8 mg/g at room temperature. Equilibrium data were fitted to Freundlich, Langmuir, and Tempkin isotherm models[83]. The Langmuir isotherm model demonstrated excellent applicability with a determination coefficient (r^2) of 0.990, indicating a monolayer capacity of 106.5 mg/g. Kinetic analysis using pseudo-first-order (PFO), pseudo-second-order (PSO) equations, and intraparticle diffusion (IPD) models suggested that chemisorption is the rate-limiting step, with the PSO model yielding an r^2 value of 0.999 and a PSO adsorption rate constant of 0.070 g/mg min. Interestingly, the presence of additives like electrolytes (Na_2SO_4 and Na_2CO_3) and surface-active agents (anionic SDS, cationic CTAB, and non-ionic Triton X-100) led to reduced dye retention compared to systems without these additives. Furthermore, the introduction of the anionic DY dye in the colloidal suspension of ST20 oxide particles significantly increased the solid surface charge density. In systems with mixed adsorbents (dye-surfactant and dye-salt), specific alterations in surface properties were observed, with the cationic surfactant having the most pronounced effect on the type and concentration of solid surface group[83].

Eman. A Allabad 2023 [84] focused on the development and characterization of *Nano bentonite* for the removal of Direct Yellow (DY), a harmful organic pollutant. Various experimental conditions, including pH, dosage, temperature, contact time, and initial DY50 concentrations, were examined. The results demonstrated that Nano bentonite achieved an impressive 94% removal rate at an initial concentration of 40 mg/L, with optimal conditions at pH 3, a dosage of 0.05 g, and a 4-hour treatment at 30°C. The adsorption process followed pseudo-second-order kinetics and the Langmuir isotherm model, indicating chemisorption interactions. Thermodynamic analysis revealed an exothermic reaction. Overall, this study strongly

recommends the use of Nano bentonite for efficient DY removal from aqueous solutions, offering a promising solution to water quality challenges in developing nations [84].

2.3.2 Bifenthrin

SBA Ghani [85] 2019 proposed the research which was to examine the efficacy of ozone treatment for removing bifenthrin from palm dates. The water treatment resulted in a 4.59% decrease in bifenthrin concentration after 15 minutes. However, after 60 minutes, it dropped by 37.24 percent. At every time point examined, ozone treatment was more effective than water treatment at removing bifenthrin. Ozone treatment for 60 minutes resulted in a 58.73% reduction in bifenthrin. This was a significant boost of around 20% compared to simply treating the water [85].

This research also discovered that ozone's effectiveness in neutralizing bifenthrin was greatly improved when metal ions were included in the treatment. The highest percentage of reduction (84.27%) was achieved with copper ions. The addition of ferrous ions enhanced elimination by 69.41%, whereas the addition of zinc ions had a moderate effect, decreasing the amount by 72.06%. Interestingly, zero valent iron (Fe⁰) reduced the efficiency of ozonated water, leading to a 44.16% reduction in bifenthrin elimination [85].

In another research by *Mixing Zhang*, [86] 2019 Bifenthrin was successfully removed from water samples using a mesoporous KIT-6-magnetite composite (Fe₃O₄@SiO₂@KIT-6). This composite was used as an adsorbent for magnetic solid-phase extraction of bifenthrin after extensive analysis. It was found that using acetonitrile as the eluent, adsorbing bifenthrin onto 40 mg of Fe₃O₄@SiO₂@KIT-6 in 100 mL water samples at pH 7, and extracting the mixture for 10

minutes yielded the best results. The detection threshold for bifenthrin was determined to be 0.005 103 mgL⁻¹ in the laboratory [86].

Experiments on the kinetics of the adsorption process showed that it followed a pseudo-second-order model, which is indicative of fast removal. Furthermore, the isotherm data fit well with the Langmuir isotherm model, demonstrating the composite's advantageous adsorption capabilities for bifenthrin[86]. As a result, this method provided a straightforward, eco-friendly, and successful strategy for detecting bifenthrin's low concentrations in environmental monitoring samples.

Abdel Hamid Bakka in 2020 [87] investigated the application of Treated Patellidae Shells (TPS) as a sorbent material in a fixed bed column for the purpose of bifenthrin removal. This research contributes to the understanding of waste valorization, the development of environmentally friendly sorbents, and the effective removal of bifenthrin pesticides. The TPS sample was subjected to characterization, revealing its composition as a singular phase of calcium carbonate (CaCO₃) with a notable high specific surface area measuring 158 m²/g.

The study investigated various important variables, such as flow rate, bed height, particle size, and bifenthrin concentration, and found that increasing these factors resulted in enhanced column efficiency. The maximum adsorption capacity of 40.53 mg was attained by employing certain parameters, including a flow rate of 8 mL/min, a bed depth of 4 cm (equivalent to 1.6 g), TPS particle size ranging from 50 to 100 μm, and a bifenthrin concentration of 20 mg/L.[87] Various mathematical models, including Bohart-Adams, Thomas, and Yoon-Nelson, were employed to examine the experimental data. Additionally, the Chu logistic model was formulated to offer a reliable fit, demonstrating superior Adjusted R-squared values and reduced χ -squared

values. This model facilitated the computation of precise parameter values based on the remaining models. The findings of this study also demonstrated that the Langmuir isotherm model accurately characterized the adsorption data, suggesting that TPS exhibits favorable adsorption characteristics and a substantial capacity for adsorbing bifenthrin.

Moreover, the study found that TPS had a notable ability to regenerate, indicating its potential efficacy in the recycling of pesticides throughout removal procedures. In general, it can be concluded that TPS demonstrated efficacy as a viable substitute for commercially available adsorbents in the context of pesticide removal from water sources[87].

2.3.3 Dioctyl Phthalate

A few physical methods for the removal of Dioctyl phthalate from literature are discussed below:

In a 1974 study *GM Carmignani* efficiency of various filter media in the removal of organic pollutants from water inside closed aquaculture systems was observed. A particular filter medium was introduced, consisting of 778 cm³ of polyurethane foam based on ether, with an ether content of 81%.[88] The exceptional properties of this particular medium were showcased through its remarkable performance, successfully removing 98.6% of a significant quantity of dioctyl phthalate (DOP), amounting to 76,545 µg (306 ppm), when subjected to a specified flow rate of 100 ml/min [88].

One noteworthy feature of this particular filter medium lies in its inherent versatility, as it possesses the capability to seamlessly integrate into a wide range of filtering systems. In addition, this material provides the advantage of reusability since it can be effectively cleaned and readied for further usage by the utilization of an acetone-hexane solution passed through the polyurethane foam. This study introduces a highly effective and adaptable approach for eliminating organic

contaminants in enclosed aquaculture systems, offering promising prospects for water treatment and the preservation of water quality [88].

The research by *Francesca Vannuchi* 2019 [89] focused on examining the potential of the "Villafranca" clone of *Populus alba* L., which is recognized for its capacity to absorb and store organic pollutants, in addressing the environmental consequences of dioctyl phthalate (DOP). *Populus* plants were cultivated hydroponically over a period of 21 days, during which they were exposed to different concentrations of d4-DOP (0, 40, and 400 $\mu\text{g L}^{-1}$).

The plants that were subjected to a concentration of 400 $\mu\text{g L}^{-1}$ d4-DOP for a duration of 21 days exhibited a significant rise in the dry biomass of their roots (+29%), while experiencing a decrease in the biomass of their aerial parts (-8%), as compared to the control group. The observed enhancement in root development was concomitant with an increase in the absorption of magnesium (Mg) by poplar trees. The LC-MS/TS analysis provided confirmation of the uptake and accumulation of d4-DOP in the roots starting from the first day of exposure. However, it should be noted that there was some detected volatilization of d4-DOP from the nutrient solution. Furthermore, a chemical interaction took place between d4-DOP and zinc (Zn) inside the root systems of plants that were subjected to elevated concentrations of d4-DOP. However, this contact did not have a restrictive effect on the accumulation of zinc in the leaves [89]. In general, this research emphasizes the notable tolerance of the "Villafranca" clone to xenobiotics and proposes that poplar trees possess the ability to absorb and store d4-DOP at the root level. This finding indicates that poplar trees have the potential to be considered as a viable option for reducing the environmental persistence of these substances [89].

2.4 Metal Oxide

Numerous dye adsorbents, such as activated carbon, red mud [90], plant residues, zeolite,[91] activated carbon aerogels, graphene oxide[92], and multi-wall carbon nanotubes, have been studied. Common adsorbents have disadvantages including high cost, minimal adsorption, and slow reaction rates. When adsorbents have sufficient active sites and a large surface area, they exhibit excellent adsorption of pollutants and a high removal capacity, as is the case with activated carbon[93].

Due to the quantum size effect and a large surface area, metal oxide NP adsorbents have several advantages, including specificity and high capacity [94, 95]. In addition, metal oxide nanoparticles (NPs) have distinct structures, varying pore sizes, and low solubility, and can be synthesized using simple, low-cost techniques [94]. Metal oxides are among the finest adsorbents due to their low solubility, robust mechanical structures, and exceptional stability against organic pigments under varying conditions [96].

Due to the prospect of complex formation interactions, metal oxides have significant applications in organic dye adsorption. Variable preparation routes with comparatively high yield, reusability, and mixing with rapid adsorption time are used to produce metal oxides.[97] In addition, metal oxides serve as both adsorbents and disinfectants in the chemical and biological treatment of the wastewater [98].

Some of the metal oxide nanoparticles according to literature are discussed below

2.4.1 Titanium Oxide

According to literature, TiO₂ nanoparticles are versatile adsorbents in various applications. TiO₂ nanoparticles offer several advantages, including cost-effectiveness, superior thermal and

chemical stability, light stability, and minimal toxicity to humans [99, 100]. These nanoparticles possess strong adsorption capabilities, a developed surface area [101], and resistance to acidic and alkaline conditions. Their surface features a high concentration of hydroxyl groups (-OH), facilitating the absorption of contaminants from water [102].

Research has explored their use in diverse areas, with a focus on photocatalytic activities. However, their potential as adsorbents has been comparatively underexplored. Notably, studies have demonstrated their effectiveness in adsorbing various pollutants from aqueous solutions. For instance, Fazal et al. (2020) [103] developed a hybrid macro algae-based biochar-TiO₂ composite for the removal of Malachite green (MG) color, exhibiting significantly improved adsorption capacity compared to pure TiO₂. Similarly, [104] Binaeian et al. (2020) used TiO₂-PAM-CS to absorb Sirius yellow K-CF dye, achieving high adsorption capacity [105]. Karim et al. (2020) prepared MWCNTs/TiO₂ nanocomposites, which outperformed pure MWCNTs in the removal of cyanide and phenol.

Furthermore, TiO₂-based nanocomposites have been employed in addressing environmental concerns. Elbarbary and Gad (2021) [106] used TiO₂/SiO₂ Nano powder to enhance the removal of basic blue 3 dyes (BB3) and Cu (II) ions from aqueous solutions. Awed et al. (2020) [107] explored the adsorption of Pb(II) and Cd(II) ions using TiO₂/kaolinite nanocomposites. Jena et al. (2019) [108] developed TiO₂-SiO₂-sulfur Nano hybrid materials for methylene blue (MG) removal. Abdul Hameed et al. (2019) [109] utilized chitosan-based CS-EGDE/TNP composites for efficient adsorption of reactive orange 16 (RO) dye.

Moreover, researchers have investigated TiO₂ nanoparticles in diverse forms and compositions. Mironyuk et al. (2019) [102] explored mesoporous carbonated TiO₂ nanoparticles for Sr(II) ion removal. Herrera-Barros et al. (2020) demonstrated the modification of biomass with

TiO₂ nanoparticles for enhanced nickel ion removal. Sharma et al. (2019) [110] manufactured mesoporous ZnO and TiO₂@ZnO nanoliths for Pb(II) and Cd(II) ion adsorption. Zain et al. (2021) [111] developed AC/TiO₂ composites with improved ruthenium N-3 dye removal.

Additionally, Chang et al. (2021) [112] synthesized MnFe₂O₄@TiO₂-rGO nanocomposites for the removal of ciprofloxacin (CIP) and Cu²⁺ from water, showcasing their potential in water purification. Zhou et al. (2021) [113] created GO-TiO₂ composite materials for efficient Cr³⁺ adsorption in wastewater

Table 2.1 Adsorption capacity of TiO₂ against different adsorbates

Adsorbent	Adsorbate	Adsorption capacity (mg/g)	Applied conditions	References
CS-EGDE/ TiO ₂	RO dye	1,407.4	Adsorbent dosage = 0.02 g.	[114]
			Adsorbate solution = 50 mL.	
			Temperature = 40 °C.	
TiO ₂ -PAM- CS	Sirius yellow K-CF dye	1,000	Adsorbent dosage = 0.05 g.	[109]
			Temperature = 40 °C.	
			Contact time = 90 min.	
			Reusability = 6 consecutive cycles.	
TiO ₂ @ZnO monolith	Pb(II) Cd(II)	978 786	Adsorbent dosage = 0.2 g/L.	[116]
			Temperature = 30 °C.	
			Contact time = 150 min.	
			pH = 6.	
			Reusability = up to 3 consecutive cycles.	
TiO ₂ .SiO ₂ - Sulfur	MB dye	804.80	Adsorbent dosage = 0.4 g/L.	[113]
			Dye solution volume = 50 mL.	
			pH = 7.	
			Reusability = 7 consecutive cycles.	
AC/TB	N-3 dye	523	Adsorbent dosage = 10 mg.	[119]
			Contact time = 180 min.	
			Removal efficiency = 99%	

2.4.2 Zinc oxide Nanoparticles

Zinc oxide (ZnO) nanoparticles are highly effective adsorbents due to their attributes such as high surface area [114] stability, [115] biocompatibilities, cost-effectiveness, and exceptional removal capacity. They exhibit a unique capability for removing anionic organic compounds, making them applicable across various fields. Several studies have explored their potential in adsorption:

Primo et al. synthesized ZnO nanoparticles using eco-friendly methods for the removal of Cu(II) ions. Zn-AL and Zn-ST showed maximum adsorption capacities of 20.42 mg/g and 10.95 mg/g, respectively, following the Langmuir isotherm.[116] Gu et al.[117] employed ZnO nanoparticles for dental purification treatment, achieving a maximum adsorption capacity of 88.547 mg/g for Cr(II) ions, following the Langmuir isotherm and PSO kinetics. Muinde et al. [118]developed chitosan–zinc oxide (CS-ZnO) nanocomposites for the removal of malachite green (MG) dye, with a maximum adsorption capacity of 11 mg/g, following the Langmuir isotherm and second-order kinetic model.

Debnath et al. [119]used ZnO nanoparticles synthesized from *Hibiscus rosa-sinensis* leaf extract to remove Congo red (CR) dye, achieving a maximum adsorption capacity of 9.615 mg/g, following the Langmuir isotherm. Nayak et al. synthesized ZnO nanoparticles from Tulsi leaf extract (ZnO-T) for the removal of Congo red (CR) dye, demonstrating a higher removal capacity (97%) than commercially available ZnO, with a maximum adsorption capacity of 74.07 mg/g, following the Langmuir isotherm.

Mittal et al.[120] utilized a self-template approach to synthesize ZnO nanoparticles for the removal of MG dye, achieving a maximum adsorption capacity of 766.52 mg/g with high adsorption efficiency.

Table 2.2 Adsorption capacity of ZnO₂ against different adsorbates

Adsorbent	Adsorbate	Adsorption capacity (mg/g)	Applied conditions	References
Zn-AL	Cu(II)	20.42	Contact time = 20 min.	[122]
Zn-ST		10.95	Initial adsorbate concentration > 80 mg/L	
ZnO	Cr(III)	88.547	Adsorbent dosage = 1 g/L.	[123]
			pH = 3.	
			Contact time = 20 min.	
			Initial adsorbate concentration = 20 mg/L	
CS-ZnO	MG dye	11	Adsorbent dosage = 0.6 g.	[124]
			pH = 8.	
			Initial adsorbate concentration = 2.3 mg/L.	
			Contact time = 180 min.	
ZnO-T	CR dye	74.07	Adsorbent dosage = 0.2 g/L.	[125]
			pH = 4.	
			Contact time = 30 min.	
			Initial adsorbate concentration = 40 mg/L	
A-Cl-PAM/ZnO	MG dye	766.52	Adsorbent dosage = 0.4 g/L.	[126]
			pH = 7	
			Contact time = 60 min.	
			Temperature = 25°C.	
			Reusability = 10 consecutive cycles.	

2.5 Problem Statement:

When the water pollutants like bifenthrin, direct yellow dye, and DOP come in contact with human beings, cause severe health hazards and diseases. Zinc oxide and titanium oxide are being used for the removal of certain water pollutants but none of them is extracting all three pollutants,

BF, DYD, and DOP, a major concern for a sustainable environment that had not been investigated and addressed. The removal through cost-effective adsorbent to adsorb the maximum number of pollutants was a need to be discovered.

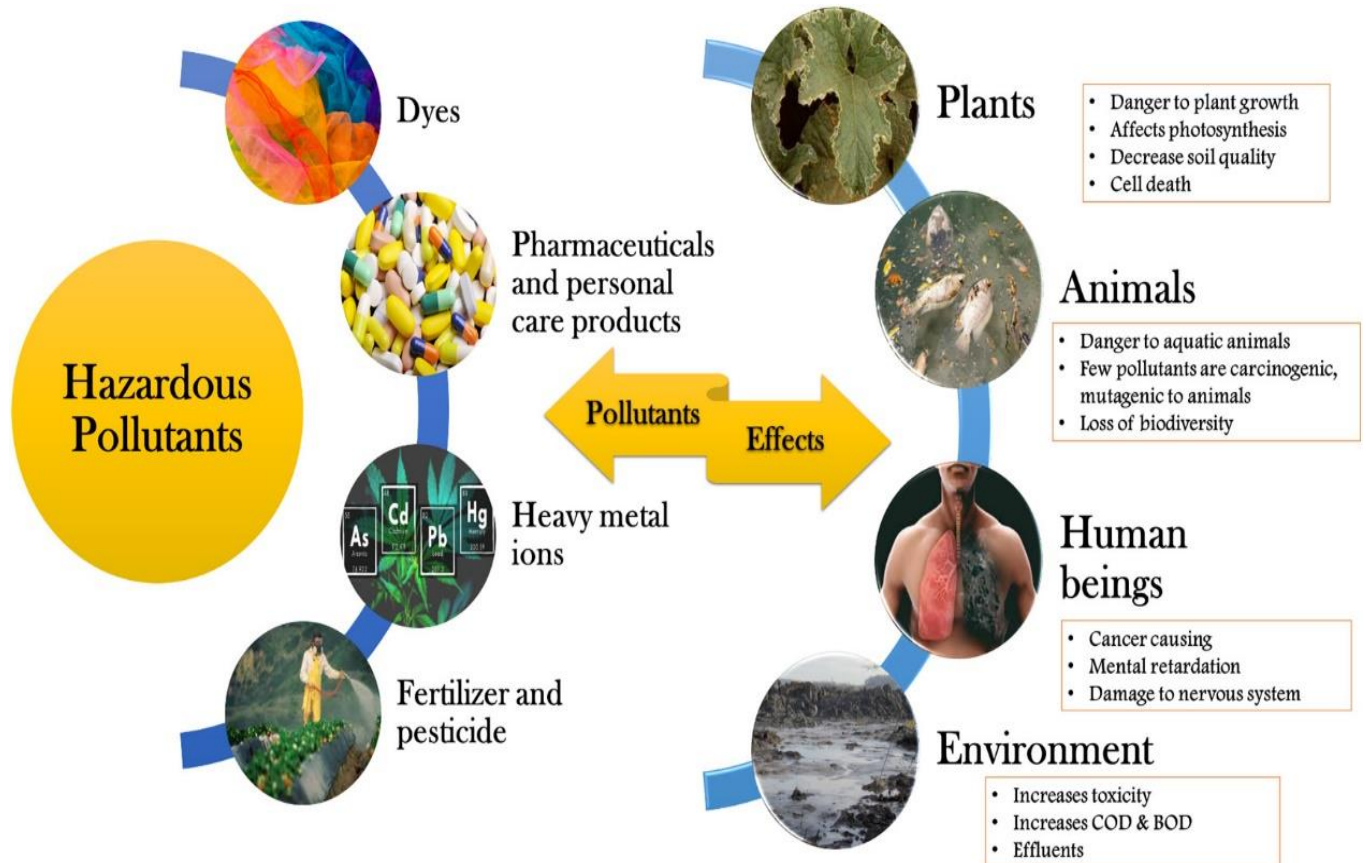


Figure 2.2 pollutants and their side effects[121]

2.6 Objectives

The main objectives of the current research are as follows:

1. Adsorption of copper oxide nanoparticles to remove coloring dye (Direct yellow dye), Pesticide (Bifenthrin), Plasticizer (Diocetyl phthalate).
2. To identify the nature of these pollutants (DYD, DOP, BF) adsorption on copper oxide (CuO) molecular sieves physisorption or chemisorption.

Chapter 3 Methodology

The aim of this research to perform an atomic/molecular level investigation to closely observe the possible sites for adsorption of (Direct yellow dye, Dioctyl phthalate, and bifenthrin) to adsorbate i.e. CuO NPs.” To carry out this aim following steps were opted

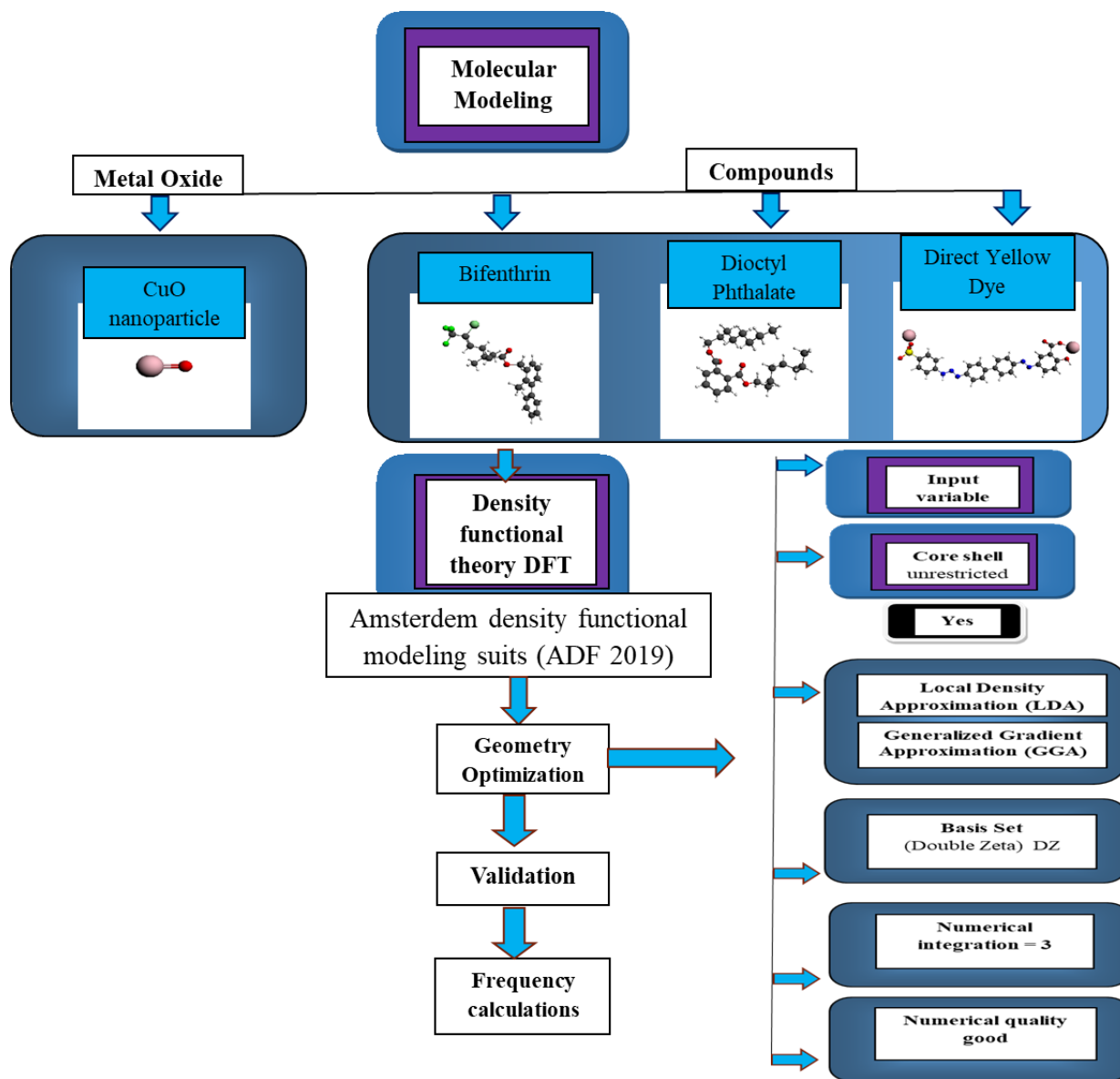


Figure 3.1 Methodology flow chart for computational modeling

Computational chemistry is an interdisciplinary discipline that uses computer science to solve chemical problems. Theoretical chemistry itself incorporates statistical techniques with basic laws of physics to atomically formulate the behavior of matter. The current work is focused to explore the adsorption approach of the three components of water over CuO using density functional theory (DFT). Quantum mechanics give us all the data related to electronic structure and the corresponding properties of a molecule that can be directly derived from wave function which is obtained by solving the time-independent Schrodinger Wave equation for a multinuclear and multi-electron system[122].

$$\hat{H} \Psi = E\Psi \quad (3.1)$$

Where ‘ Ψ ’ is the many electrons wave function, E is the Eigenvalue of the operator (total energy of the system) and H is the called Hamiltonian operator and is equal to the sum of kinetic and potential energy operator as

$$\hat{H} = T + V \quad (3.2)$$

3.1 Computational Software:

In the field of computational chemistry, there exists a diverse array of software options that are accessible both within academic institutions and through commercial platforms. The software packages employed in this research include ADF (Amsterdam Density Function Modelling Suite) 2019.304, which was utilized for conducting Density Functional Theory (DFT) computations.

3.2 Amsterdam Density Functional (ADF) Software

The Amsterdam Density Functional-ADF_2019.304 is a computational software package used in the field of quantum chemistry. The ADF program is widely utilized in the field of computational

chemistry due to its exceptional computing efficiency in conducting Density Functional Theory (DFT) investigations. The program in concern is a modelling and simulation software created by AMS (Amsterdam Modelling Suite). It encompasses various packages such as ADF, BAND, UFF, ReaxAms, ReaxFF, Quantum Espresso, DFTB, among others. The ADF software package is primarily employed for doing calculations based on the Density Functional Theory (DFT), classical Molecular Dynamics (MD) simulations, and other characterization techniques such as Thermodynamics, UV/IR/XAS/NMR/ESR Spectra, and Frequencies. This software also allows for the application of Semi-Empirical and Ab-Initio methods, which have demonstrated excellent levels of accuracy. This software finds benefit in various domains such as chemistry, bio-medical sciences, and material sciences, among others.

3.3 Density Functional Theory (DFT) Studies:

Density Functional Theory (DFT) study is an advanced approach that allows the detailed analysis of complexities that cannot be visualized experimentally. ADF 2019.304 is an excellent software to perform DFT studies on bioorganic, inorganic, organo-metallic, metal complexes, and other material-based molecules/ions.

The energy in DFT consists of the following six major components;

$$E_{\text{DFT}} = E_{\text{NN}} + E_{\text{T}} + E_{\text{V}} + E_{\text{Coulomb}} + E_{\text{Exchange}} + E_{\text{Correlation}}$$

Here, E_{NN} is nuclear-nuclear repulsion, E_{V} is nuclear-electron attraction, E_{T} is the kinetic energy of electrons, E_{Coulomb} is the classical electron-electron Coulomb repulsion, E_{Exchange} is the non-classical electron-electron exchange energy which is different from Hartree-Fock theory and $E_{\text{Correlation}}$ is correlated to the movement of electrons with different correlations and this is also different from the Hartree-Fock theory.

The DFT method is primarily based on the Schrodinger wave equation (Ψ) for quantum mechanical treatment of a system. The main feature of the DFT study is to resolve the ground state energy of any system. DFT follows Hohenberg-Kohn equation and Kohn-Sham equation. Utilizing this basic equation there are many functional developed are called Density Functional or Exchange-Correlation (XC) Functional. These functional includes LDA (Local Density Approximation), GGA (Generalized Gradient Approximation), hybrid-GGA, meta-GGA, etc.

The LDA is the simplest approximation and is usually applied to gas phase simulations. LDA is a direct representation of the original Kohn and Sham equation for ground state energy calculation. With the advancement of algorithm and correction in previous LDA functional, the GGA is highly recommended for DFT calculations. GGA has a variety of forms and shows diversity in hybrid and meta-functional forms. GGA utilizes both LDA's density and its gradient at each point in simulation and is significantly more accurate than LDA. The famous GGA-Functional includes PBE, BLYP, PB86, and PW91. The PW91 (developed by Perdew-Wang in 1991) is highly recommended for nano-molecule optimization. BLYP (developed by Burke-Lee-Yang-Parr in 1988) and PBE (developed by Perdew-Burke-Ernzerhof in 1996) is recommended for organic, inorganic, bio-molecule, metal, and organo-metallic molecule. The hybrid-GGA i.e. B3LYP has some combination of GGA with Hartree-Fock exchange. The meta-GGA i.e. TPSSh additionally depends upon the Kohn-Sham kinetic energy density.

3.3 Taxonomy for function

- 1) All practical functionals are approximations.
- 2) Currently, no functional is extremely accurate for all attributes of interest.
- 3) Any functional can be used for any electronic structure problem without additional input.

Functional differs from simple to complex

We used GGA-PW91 to find the best results for our research.

3.3.1 GGA Functional

(GGAs) produces an accuracy which is useful in chemical calculations and applicable for extended systems (Materials). As my work is based on the application of nanoparticles copper oxide there for we have performed DFT method with GGA approximations implemented in ADF software to investigate electronic structure, geometric stability, adsorption constant and spectral behavior of nanoparticle copper oxide. GGA has a variety of forms and shows diversity in hybrid and meta-functional forms. GGA utilizes both LDA's density and its gradient at each point in simulation and is significantly more accurate than LDA. The famous GGA-Functional includes PBE, BLYP, PB86, and PW91. The PW91 (developed by Perdew-Wang in 1991) is highly recommended for nano-molecule optimization. BLYP (developed by Burke-Lee-Yang-Parr in 1988) and PBE (developed by Perdew-Burke-Ernzerhof in 1996) is recommended for organic, inorganic, bio-molecule, metal, and organo-metallic molecule. The hybrid-GGA i.e. B3LYP has some combination of GGA with Hartree-Fock exchange. The meta-GGA i.e. TPSSH additionally depends upon the Kohn-Sham kinetic energy density.

3.3.2 Basis Set

A mathematical description of the molecular orbitals of a system, which is used for an approximate theoretical calculation or modeling is called a basis set. It is treated as a set of basic building blocks that can be added to acquire required features. In the present work we have applied DZ basis set using LDA and GGA: PW91 functional to optimize all prescribed structures.

3.3.3 Double Zeta Basis set

The function with smaller zeta calculates the charge distribution at larger values of the nucleus while the large zeta only finds charge near to the nucleus. This expanded basis set is known as double zeta basis set. The orbitals of chemically inequivalent molecules are considered of same type without the use of double zeta basis set. For example, in acetylene the pz orbital along the inter nuclear axis is in a quite different chemical environment and different bonding than the px and py orbitals. By using double zeta basis set the pz orbital is not constrained to be the same size as the px and py orbitals.

Table 3.1 Parameters for the DFT studies of CuO NP and the waste water pollutants.

Compounds	Task	XC-Functional	Basis Set	Charge Spin Polarization
CuO NP	Geometry Optimization & Frequency	GGA: PW91	DZ	'0' & '0'
Bifenthrin	Geometry Optimization & Frequency	GGA:PW91	DZ	'0' & '0'
Diocetyl phthalate	Geometry Optimization & Frequency	GGA:PW91	DZ	'0' & '0'
Direct yellow dye	Geometry Optimization & Frequency	GGA: PW91	DZ	'0' & '0'

GGA-PW91 was used to conduct DFT studies. Geometry optimization of CuO NP and the compounds (Bifenthrin, dioctyl phthalate) were calculated by XC functional GGA-PW91, the results were then validated using frequency calculations by using same parameters.

The adsorption energies were calculated using following formula

$$E_{\text{ads}} = E_{\text{composite}} - (E_{\text{NP}} + E_{\text{Dye}}) \quad (3.1)$$

The E_{ads} is total adsorption energy while $E_{\text{composite}}$, E_{NP} and E_{Dye} is geometry optimization energy of composite, nanoparticle and the dye(s) respectively.

Chapter 4 Results

Water pollution is currently a major issue, with sources ranging from industrial waste and deforestation to domestic waste and oil pollution etc. These sources introduce various effluents into water bodies, including heavy metals, pharmaceuticals wastes, pesticides, fertilizers, dyes, and phthalates. In this study, computational models were employed to analyze and study the extraction behavior of three major components: dyes (direct yellow dye), pesticide (bifenthrin) and phthalate (dioctyl phthalate) from wastewater by using adsorption phenomena.

4.1 Geometry optimization and electronic structure.

All model geometries of wastewater components: dyes (direct yellow dye), pesticide (bifenthrin) and phthalate (dioctyl phthalate) were initially optimized using GGA-PW91/DZ level of density functional theory method. Frequency calculations were then performed on the optimized geometries.

DFT was performed to acquire thermodynamic values i.e. Entropy, Enthalpy, and Gibbs energy for copperoxide nanoparticle and these three wastewater components: dyes (direct yellow dye), pesticide (bifenthrin) and phthalate (dioctyl phthalate). Adsorption process feasibility and spontaneity are assessed using Gibbs free energy of change. Negative value of gibbs energy ΔG indicates spontaneous and positive value of gibbs energy ΔG indicates non-spontaneous process. ΔS increase (+ve) and ΔH decrease (-ve) during the process of adsorption.

The adsorption energies were calculated using the following equation.

$$E_{\text{ads}} = E_{\text{composite}} - (E_{\text{NP}} + E_{\text{Dye}}) \quad (4.1)$$

Whereas E_{NP} is the energy of adsorbent, in this case it is CuO, E_{Dye} is the energy of the adsorbate, bifenthrin, diocyl phthalate or direct yellow dye and $E_{(composite)}$ is the energy of the complex.

DFT studies were further performed to obtain numerous critical properties like most geometry-optimized state of the structure, the HOMO-LUMO energy gaps, the adsorption energy and infrared spectra calculations.

Table 4.1 Binding energy, enthalpy, entropy of CuO NPs and (BF,DOP and DYD) before adsorption.

Parameters	Copperoxide Nanoparticles	Bifenthrin	Diocylphthalate	Direct yellow Dye
Optimization Energy eV	-3.7238	-301.3916	-371.253	-348.7579
Enthalpy (ΔH)(eV)	-3.7556	-311.3427	-378.249	-364.5438
Entropy (S)(cal/mol-K)	54.207	180.122	192.3	218.365
$\Delta G = \Delta H - T\Delta S$ (kcal/mol)	-15886.4066	-53087.0887	-56722.149	-64345.4888

4.1.1 Copper Oxide Nanoparticle

The computational results show that the copper-oxygen bond length is 1.705 Å, calculated optimized energy is -3.72 eV (Table 4.1). Frequency calculation validated the energy minimization of this geometry. This optimized geometry of CuO will be used for adsorption study (Figure 4.1).

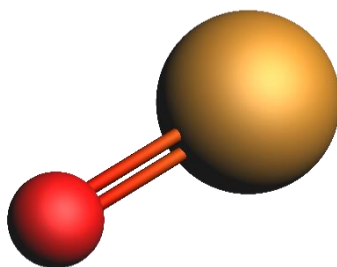


Figure 4.1 Optimized geometry of CuO nanoparticle (red ball shows oxygen atom whereas golden ball shows copper atom)

4.1.2 Bifenthrin (pesticide)

Geometry of bifenthrin was initially optimized using the same level of DFT method and then CuO was adsorbed on this optimized structure. For adsorption, two sites, center and terminal, of bifenthrin was considered (Figure 4.2). According to the optimized data, CuO makes interaction with the C=O of carbonyl group when adsorbed at the central site whereas, with the heteroatoms chlorine and fluorine when adsorbed at the terminal site.

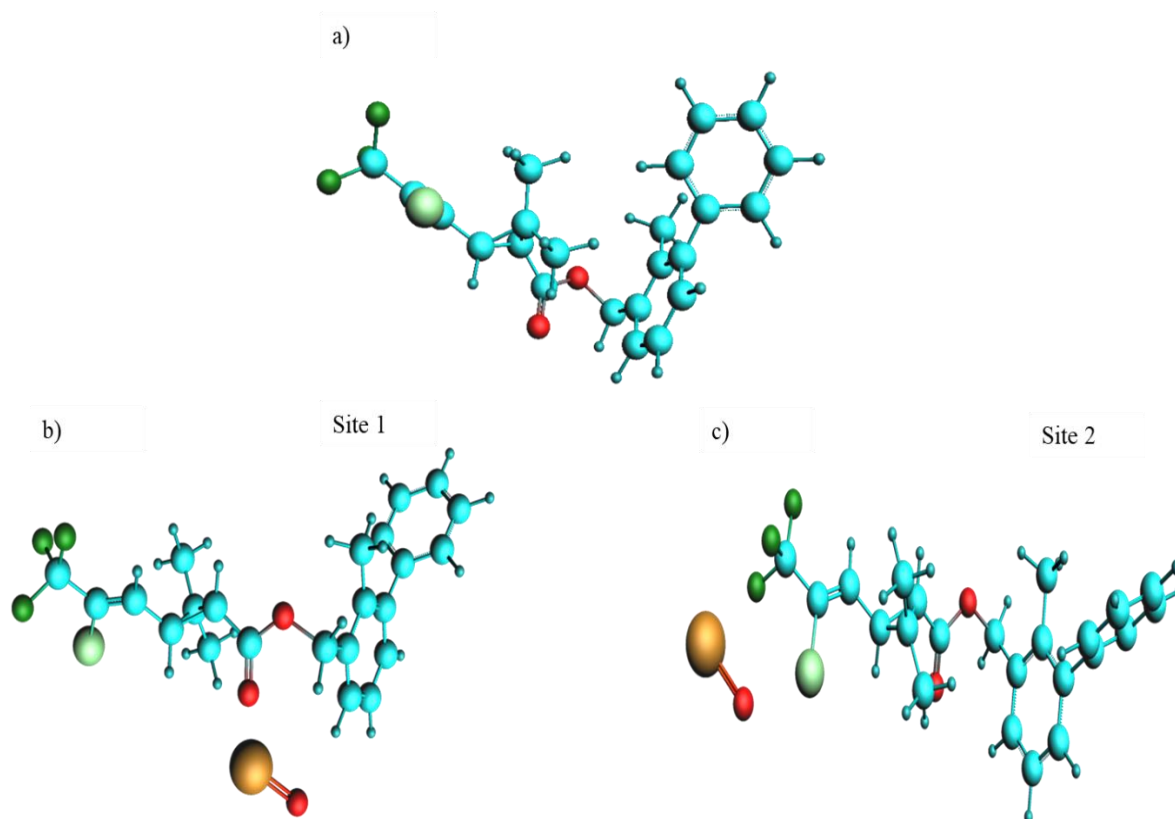


Figure 4.2 Optimized geometries of (a) Bifenthrin (light blue balls: carbon, green ball: fluorine, red balls: oxygen, small light blue balls: hydrogen, pea green balls: chlorine) (b) CuO adsorbed at the central position (c) CuO adsorbed at the terminal position

HOMO-LUMO energy gap determines the ease of electron to leave the HOMO and enters the LUMO, the lower the gap the higher possibility of the electron transition between the two molecules/atoms/ions/elements. Comparing the HOMO-LUMO energy gap between the two

geometries, it has been observed that the energy gap increases to -0.757 (eV) when CuO is adsorbed at the center whereas it is -1.334 eV when adsorbed at the terminal site. The lower the energy gap, more possibility of adsorption occur, therefore, we can say that the adsorption at the terminal sites of bifenthrin is more feasible than at the central carbonyl group.

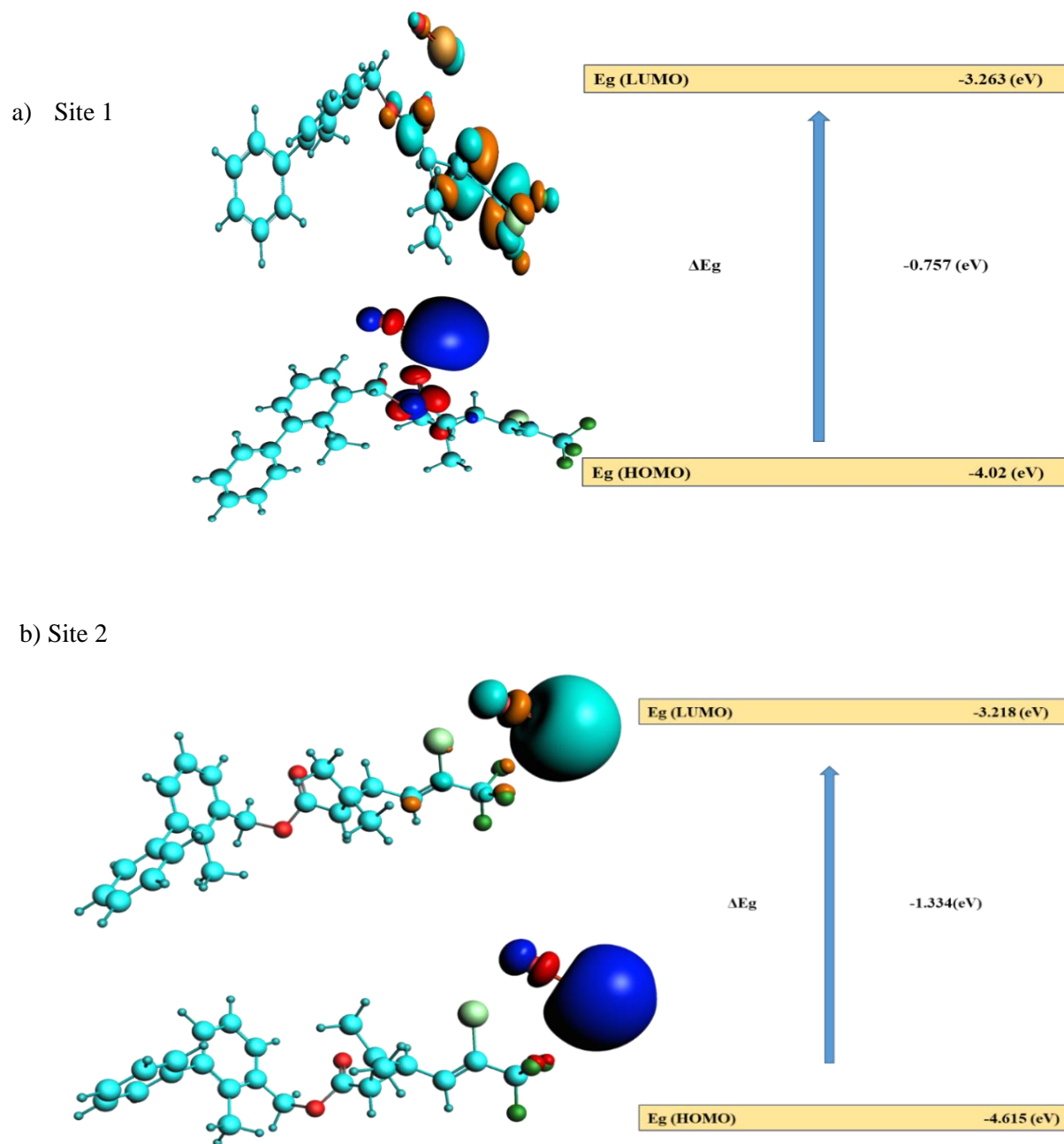


Figure 4.3 Frontier Molecular Orbitals of CuO adsorbed at the (a) Center of Bifenthrin (b) Terminal position of Bifenthrin.

The charges factor along with the atomic bond or gaps between atoms has strongly depicted which site of the molecule has potential attachment for adsorption on the surface of the CuO nanoparticles. From computed results the most suitable site for the adsorption of adsorbent to dye is at the terminal position. At the central position bond distances are smaller which makes CuO difficult to remove from the dye. Therefore, the adsorption after simulation with charges variation recommends the higher chances of physisorption between CuO NPs toward the terminal halogens of dye.

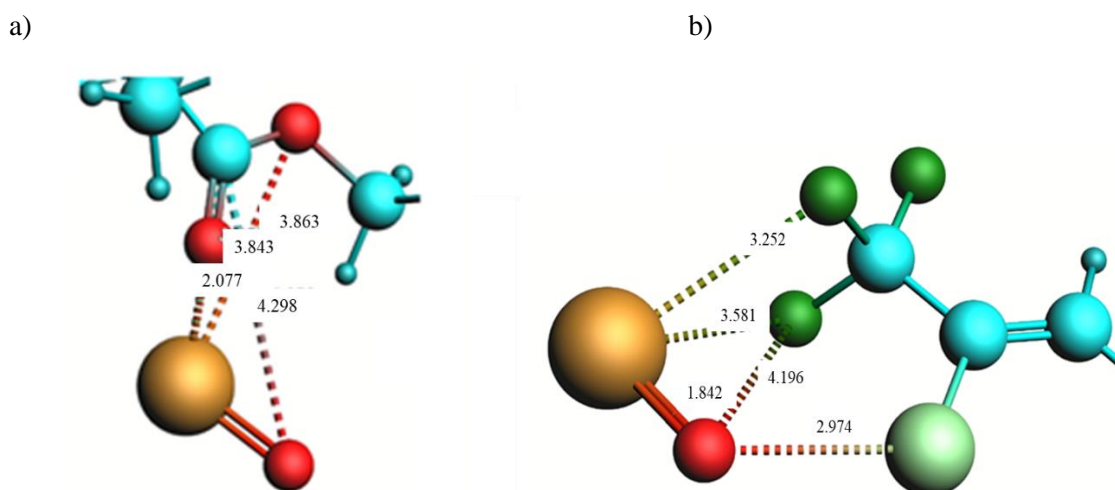


Figure 4.4 Bond Distances between CuO adsorbed on bifenthrin at the (a) Central Site (b) Terminal Site

(Golden Ball: Copper, Red Ball: Oxygen, Light Blue Ball: Carbon, Dark Green Ball: Fluorine, Pea Green Ball: Chlorine & Small blue Ball: Hydrogen).

Table 4.2 Atomic bond distance and Mulliken's charges on atoms on dye (bifenthrin) and CuO NPs.

Bifenthrin (Central Site)					
Bond Distances (Å)					
Bond Between	Cu=O (NPs)	Cu-O (O=CO)	Cu-O (C-O-C)	O-H (NP – Dye)	O-C (NP – Dye)
Before Adsorption	1.705	3.342	3.369	2.266	3.145
After Adsorption	1.836	2.077	3.843	3.038	3.979
Mulliken's Charges					
Elements	Cu (NPs)	O (Dye)	C (Dye)	O (NPs)	H (Dye)
Before Adsorption	0.301	-0.583	-0.36	-0.301	0.317
After Adsorption	0.314	-0.685	-0.375	-0.381	0.344
Bifenthrin (Terminal Site)					
Bond Distances (Å)					
Bond Between	Cu=O (NP)	Cu-Cl (NP – Dye)	Cu-F (NP – Dye)	O-Cl (NP – Dye)	O-F (NP – Dye)
Before Adsorption	1.705	3.702	3.217	3.518	3.78
After Adsorption	1.843	3.908	3.252	2.974	3.58
Mulliken's Charges					
Elements	Cu (NPs)	F (Dye)	C (= bond)	O (NPs)	Cl (Dye)
Before Adsorption	0.301	-0.343	-0.349	-0.301	0.15
After Adsorption	0.198	-0.279	-0.351	-0.241	0.183

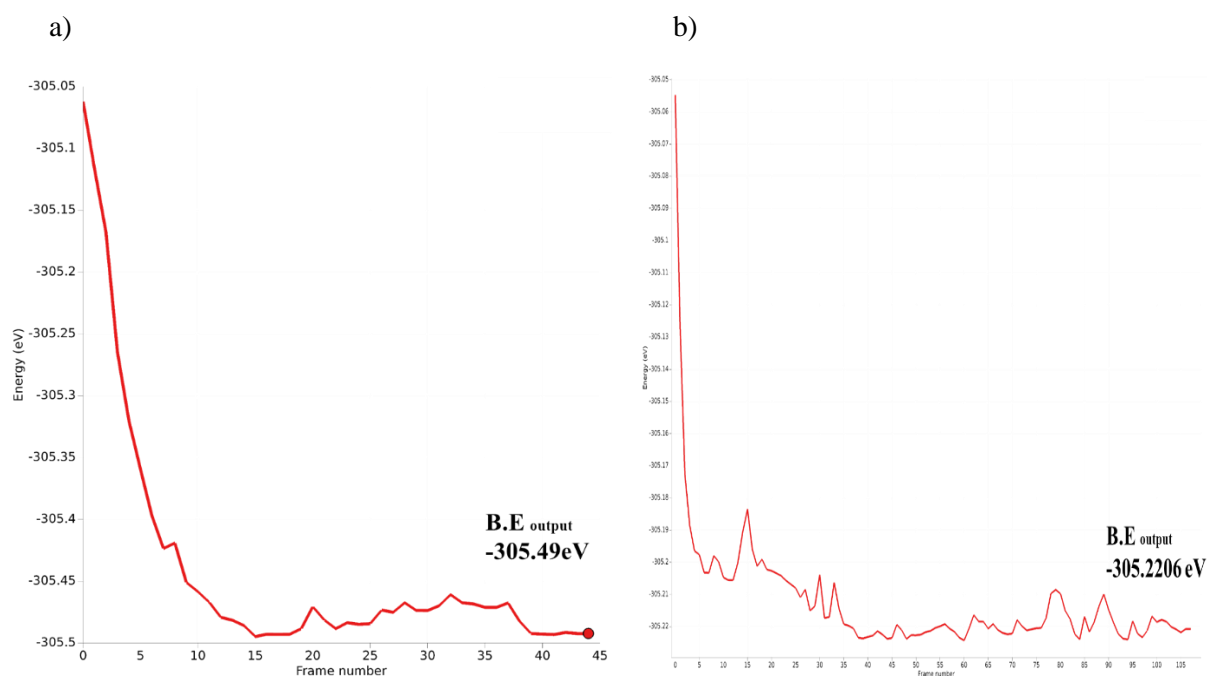


Figure 4.5 Binding energies for CuO Adsorbed at (a) Terminal position of bifenthrin, (b) Central position of Bifenthrin

The above graphs show the binding energy of Bifenthrin and CuO nanoparticle after adsorption from two different sites. In site a) the computed binding energy between the CuO with the central carbonyl of Bifenthrin is -305.062 eV, whereas Figure 4.5 (b) shows that the computed binding energy between the CuO with the terminal halogens of Bifenthrin is -305.49 eV. Comparing the binding energies, although the binding energy of CuO adsorbed at the carbonyl position is low, the binding at the terminal position is more feasible. The reason is, CuO nanoparticles are used for the waste water treatment here, which means after the removal of bifenthrin using CuO NPs, CuO will be converted again to its NPs form and will be available to use again. If the binding energy is strong between the adsorbent and the adsorbate, the retrieval of CuO NPs would be difficult. Also, the difference between the binding energies is negligible.

Table 4.3 The optimized energy values and adsorption energy values of CuO and bifenthrin before and after adsorption on two different angles.

Bifenthrin	(before adsorption)	(after adsorption) Central Site	(after adsorption) Terminal Site
Opt energy in eV on ADF	-301.3916	-305.4921	-305.2206
Enthalpy (ΔH)(eV)	-311.3427	-315.8218	-315.3384
Entropy (S)(cal/mol-K)	180.122	202.967	201.886
$\Delta G = \Delta H - T\Delta S$ T=298.15 (kcal/mol)	-53087.0887	-60,830.432	-60,507.649
$\Delta E_{adp} = -\text{composite-}$ $(NP+dye)(eV)$	----	-0.3767	-0.1052

The binding energy of Bifenthrin before adsorption was -301.3916, after adsorption it decreased to -305.4921eV and -305.2206eV for central and terminal sites, respectively. When the process of adsorption takes place the Gibbs free energy value decreases from -53087.0887 to -60830.432eV and -60507.649eV for central and terminal sites, respectively which shows the spontaneity of the process. A negative value of interaction energy (ΔG) represented the favored adsorption whereas positive value indicated the theoretically unfavored interaction of adsorbate with adsorbent. The negative values of adsorption energy show it is an exothermic process. So, if we compare the adsorption energy values adsorption at the central site shows the highest possible attraction of CuO with bifenthrin.

4.1.3 Dioctyl Phthalate

Geometry of Dioctylphthalate was initially optimized using the same level of DFT method and then CuO was adsorbed on this optimized structure. For adsorption, one terminal position, with oxygen, of dioctylphthalate was considered (Figure 4.6 b). According to the optimized data, CuO makes interaction with the C = O of carbonyl group of ester when adsorbed from terminal site.

This was accomplished by using the same GGA-PW91 parameter with a basis set double zeta. Frequency calculation validate the energy minimization of this geometry

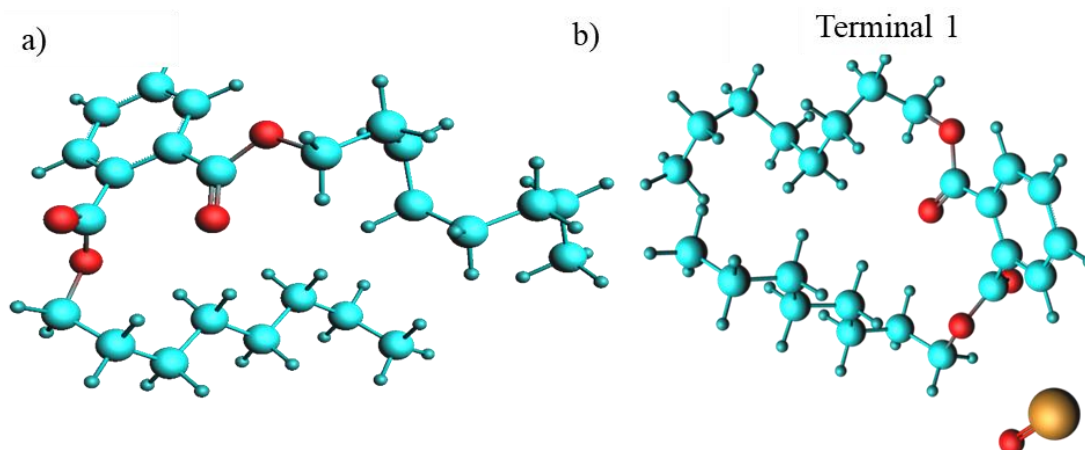


Figure 4.6 Optimized geometries of (a) Diocetyl phthalate b) CuO adsorbed at the Diocetylphthalate. (light blue: carbon, red balls: oxygen, small light blue balls: hydrogen) Diocetyl phthalate Figure 4.5 a) have oxygen(s) as a possible site for attraction or adsorption with CuO NPs. Figure 4.7 show the energy, HOMO-LUMO gap of diocetyl phthalate and CuO adsorption.

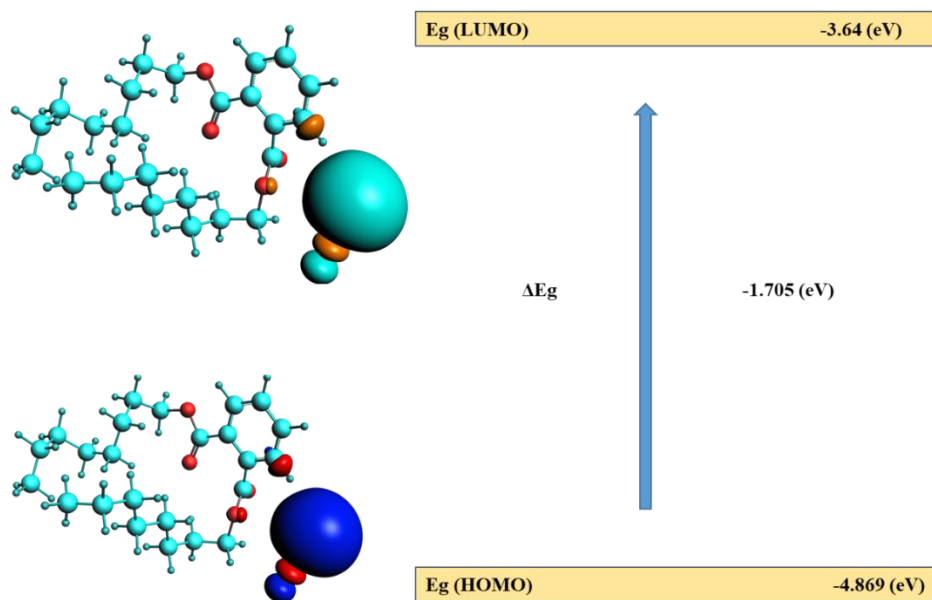


Figure 4.7 Frontier molecular orbitals of CuO adsorbed at the diocetyl phthalate

The dioctyl phthalate has carboxylic oxygens, so the attachment of CuO (NPs) is analyzed on oxygen(s) of the carboxylic group. The HOMO-LUMO energies (ΔE_g) are shown to be -1.705 (eV) in figure 4.7 (a). The following figure 4.8 and table 4.4., further provides the confirmation for possible adsorption site.

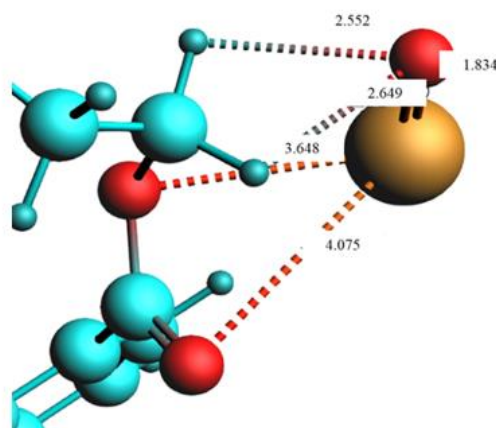


Figure 4.8 Bond distance between CuO NPs adsorbed on dioctyl phthalate at terminal position (Golden Ball: Copper, Red Ball: Oxygen, Light Blue Ball: Carbon, & Small blue Ball: Hydrogen).

Dioctyl phthalate (terminal site)					
Bond Distances (Å)					
Bond Between	Cu=O (NPs)	Cu-O (C=O)	Cu-O (C-O-C)	O-H (NP + Dye)	-
Before Adsorption	1.705	3.955	3.158	2.46	-
After Adsorption	1.834	4.075	3.348	2.649	-
Mulliken's Charges					
Elements	Cu (NPs)	O (= bond)	O (- bond)	O (NPs)	H (Dye)
Before Adsorption	0.301	-0.506	-0.489	-0.301	0.285
After Adsorption	0.289	-0.509	-0.543	-0.337	0.329

Table 4.4 The atomic bond distances and Mulliken's charges for the atoms of dioctyl phthalate dye and CuO NPs

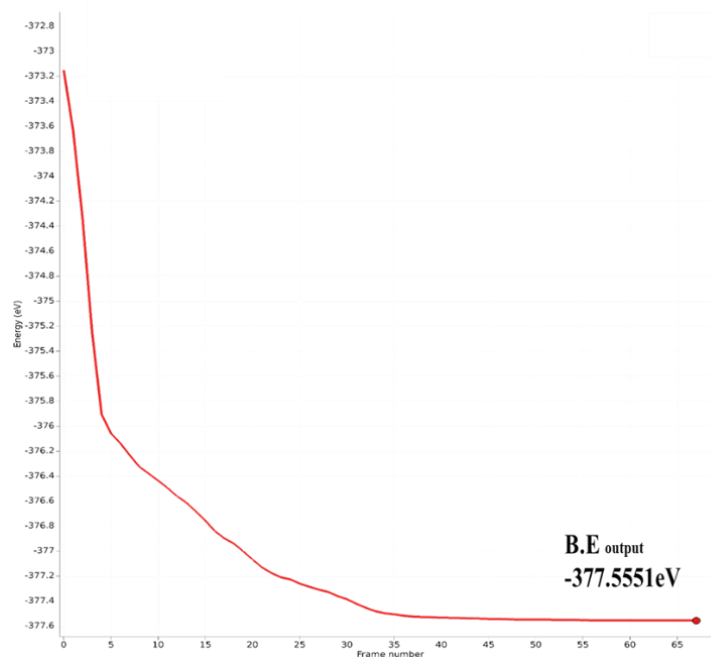


Figure 4.9 Binding energies of CuO adsorbed at two different ester group oxygen sites of Diocetylphthalate

Figure 4.9 shows the binding energy of dioctylphthalate and CuO nanoparticle after adsorption. The computed binding energy between the CuO with the oxygen of ester group of dioctyl phthalate is -377.5551 eV.

Table 4.5 The optimized energy values and adsorption energy values of CuO and dioctylphthalate before and after adsorption on two different angles.

Diocetyl phthalate	(before adsorption)	(after adsorption)
Opt energy in eV on ADF	-371.253	-377.5551
Enthalpy (ΔH)(eV)	-378.249	-384.394
Entropy (S)(cal/mol-K)	192.3	218.976
$\Delta G = \Delta H - T\Delta S$ T=298.15(kcal/mol)	-56722.149	-64,544.362
$\Delta E_{adp} = -\text{composite-}$ $(NP+dye)(eV)$	----	-2.5783

The optimized energy of dioctylphthalate before adsorption was -371.253, after adsorption it decreased to -377.5551 eV. When the process of adsorption takes place the Gibbs free energy value also decreases -56722.149 to -64,544.362 eV which shows spontaneity of the process. A negative value of interaction energy (ΔG) represented the favored adsorption whereas positive value indicated the theoretically unfavored interaction of adsorbate with adsorbent. The negative values of adsorption energy show it is an exothermic process.

4.1.4 Direct Yellow Dye

Geometry optimization was initially optimized using the same level of Density functional theory method and then CuO was adsorbed on this optimized structure. GO is done to move the atoms of molecule (direct yellow dye) to get its most stable-structure with lowest possible ground state geometry by using the parameter given in methodology with basis set double zeta (DZ).

For adsorption, there different positions, central, terminal 1 and terminal 2 of Direct yellow dye was considered due to the presence of high electronegative atoms (Figure 4.10). According to the optimized data, CuO makes interaction with the nitrogen of azo group present on the sulphonic group at central position, whereas it also shows interaction with sulphonic group at terminal 1 and carboxylic group at terminal 2. (Figure 4.10)

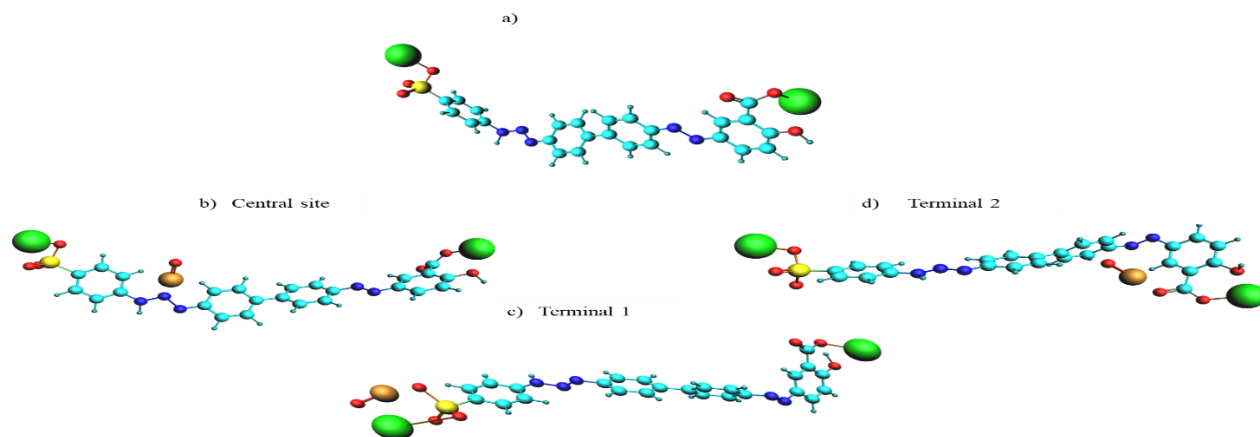


Figure 4.10 Optimized geometry of (a) direct yellow dye **b)** CuO adsorbed at the central position **c)** CuO adsorbed at terminal 1 **d)** CuO adsorbed at terminal 2. (light blue balls: carbon, Dark blue balls: nitrogen, red balls: oxygen, small light blue balls: hydrogen, green balls: sodium, yellow balls: Sulphur)

The optimized HOMO LUMO energy gap for the central site is -0.705 (eV) whereas for CuO adsorbed at the terminal 1 is -1.027 (eV) and for terminal-2 is -1.582 (eV). The computed results of HOMO-LUMO energies (ΔE_g) indicates that the most suitable site for the adsorption of adsorbent to dye is at terminal 2 position where CuO interact with the oxygen atom of carboxylic group.

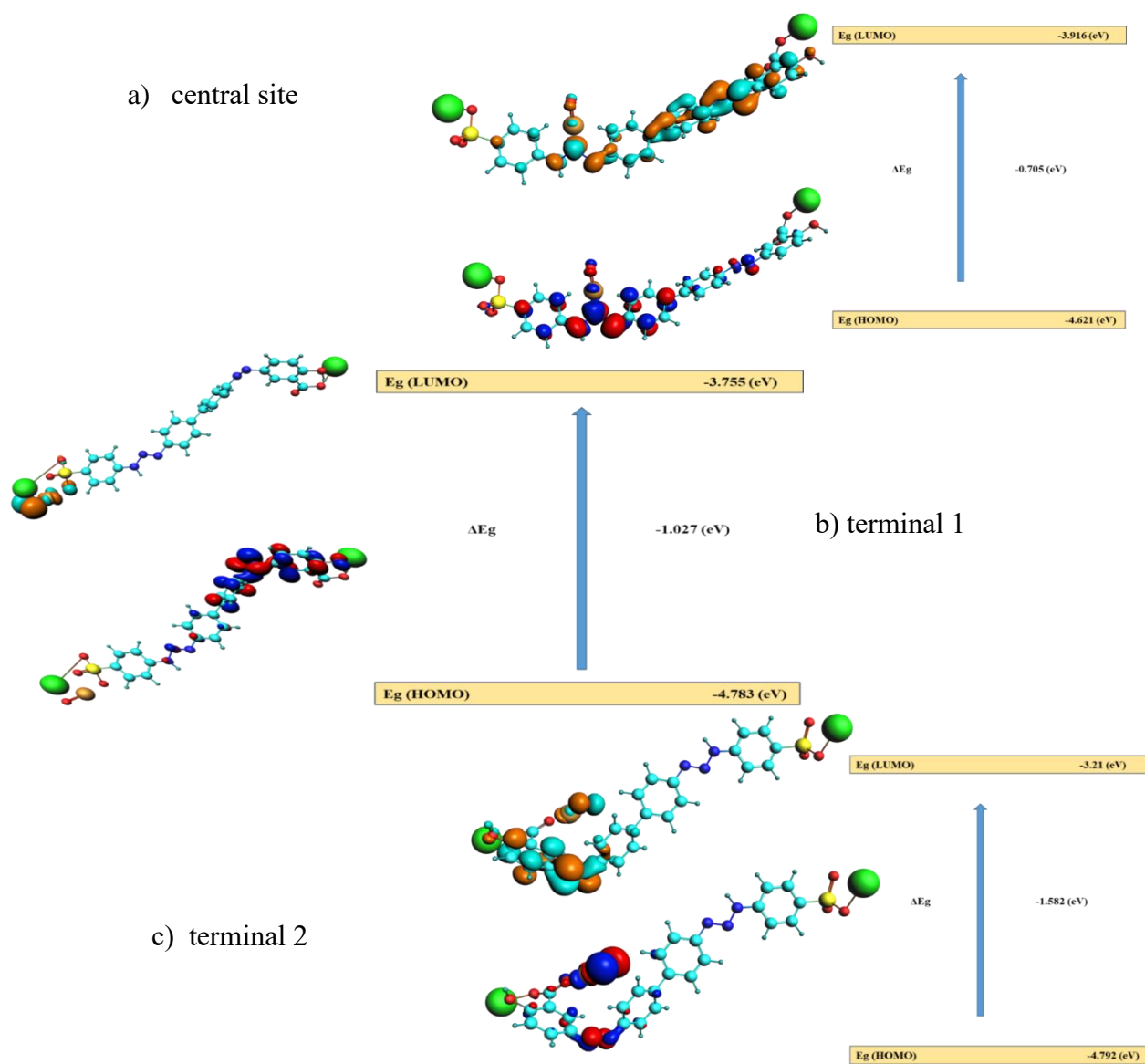
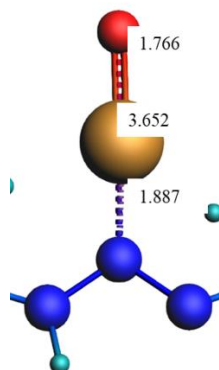
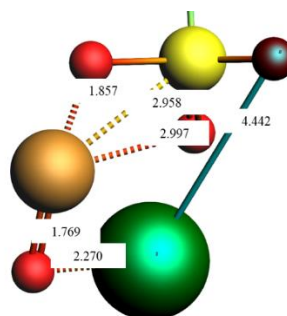


Figure 4.11 Frontier Molecular Orbitals of CuO adsorbed at the (a) Center of DYD (b) Terminal position 1 of DYD (c) terminal position 2 of DYD

a) Central position



b) terminal 1



c) terminal 2

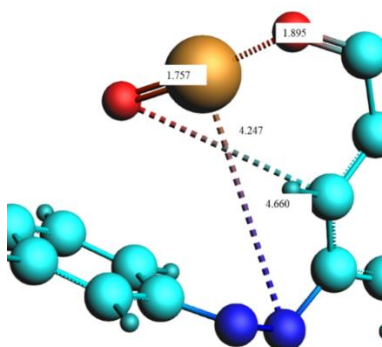


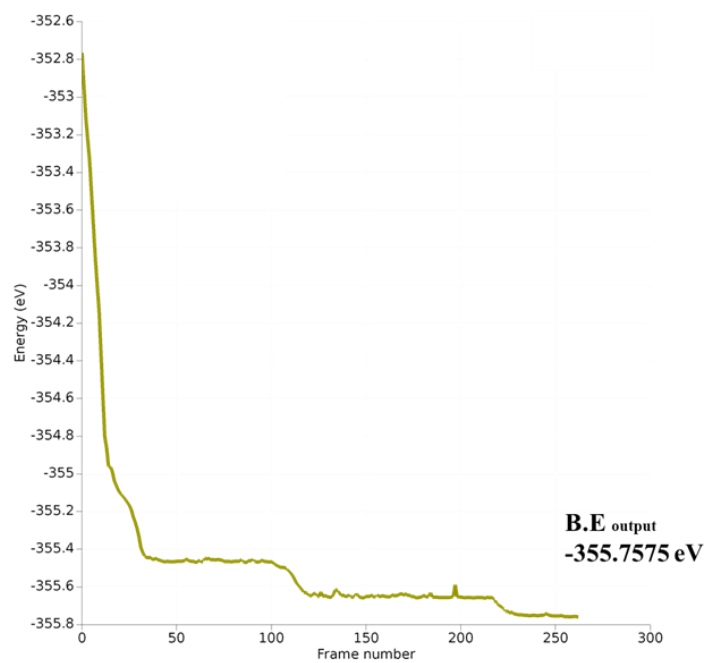
Figure 4.12 (a,b&c) Bond distance between CuO adsorbed on DYD at the (a) central (b) terminal 1 (c) terminal 2.

(Red Ball: Oxygen, Light Blue Ball: Carbon, Dark Green Ball: Fluorine, Navy Blue Ball: Nitrogen, Yellow Ball: Sulphur, Green Ball: Sodium and Small White Ball: Hydrogen).

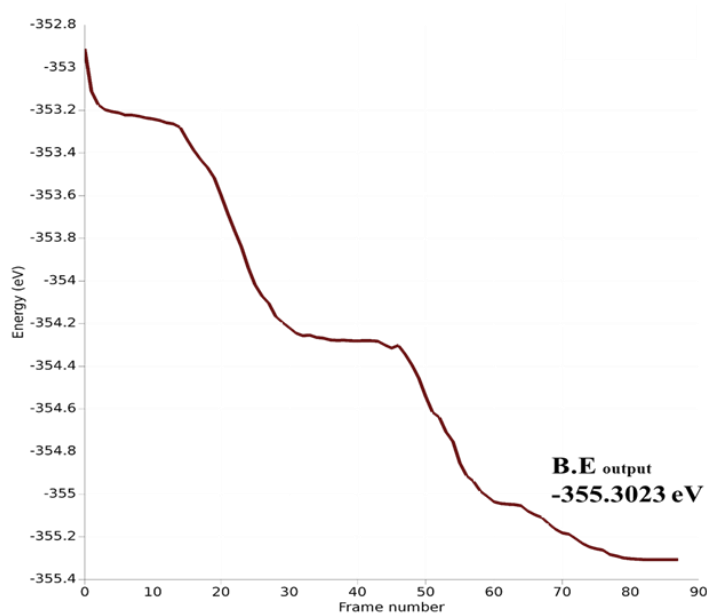
Table 4.6 The atomic bond distances and Mulliken's charges on atoms on direct yellow dye and CuO NPs.

Direct Yellow (central)					
Bond Distances (Å)					
Bond Between	Cu=O (NPs)	Cu-N (HN-N=N)	Cu-N (HN-N=N)	O-H (NP + Biphenyl)	O-H (NP + Aromatic)
Before Adsorption	1.705	2.535	2.966	2.558	3.729
After Adsorption	1.766	1.887	2.915	3.793	3.43
Mulliken's Charges					
Elements	Cu (NPs)	N (HN-N=N)	N (HN-N=N)	O (NPs)	H (Aromatic)
Before Adsorption	0.301	-0.084	-0.486	-0.301	0.324
After Adsorption	0.61	-0.346	-0.457	-0.484	0.336
Direct Yellow (terminal 1)					
Bond Distances (Å)					
Bond Between	Cu=O (NPs)	Cu-O (S=O)	Cu-O (S=O)	O-Na (NPs + Dye)	-
Before Adsorption	1.705	4.067	3.667	3.599	-
After Adsorption	1.789	1.857	2.997	2.27	-
Mulliken's Charges					
Elements	Cu (NPs)	O (S=O)	O (S=O)	O (NPs)	Na (Dye)
Before Adsorption	0.301	-0.644	-0.808	-0.301	0.892
After Adsorption	0.5	-0.712	-0.793	-0.711	0.898
Direct Yellow (terminal 2)					
Bond Distances (Å)					
Bond Between	Cu=O (NPs)	Cu-O (C=O)	O-N (N=N)	O-H (NPs + Biphenyl)	O-H (NPs + Aromatic)
Before Adsorption	1.705	5.286	4.303	6.129	4.965
After Adsorption	1.757	1.895	4.817	2.447	4.007
Mulliken's Charges					
Elements	Cu (NPs)	O (C=O)	N (N=N)	O (NPs)	H (Biphenyl)
Before Adsorption	0.301	-0.578	-0.283	-0.301	0.322
After Adsorption	0.605	-0.663	-0.267	-0.612	0.374

a) Site 1



b) Site 2



c) Site 3

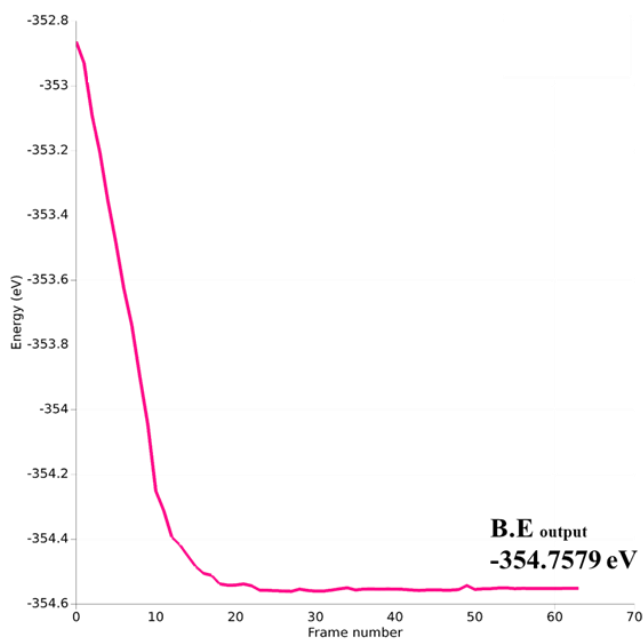


Figure 4.13 Binding energies for CuO NP adsorbed at a) central position b) terminal 1 c) terminal 2 of DYD

The above graphs show the binding energy of DYD and CuO nanoparticle after adsorption from three different sites. In site a) the computed binding energy between the CuO with the central azo nitrogen of DYD is -355.7575 eV, whereas Figure 4.13 (b) shows that the computed binding energy between the CuO with the terminal sulphonic group of DYD is -355.3072 eV, c) shows that the computed binding energy between the CuO with the terminal carboxylic group of DYD is -354.5511 eV. Comparing the binding energies, although the binding energy of CuO adsorbed at the azo nitrogen group is low, the binding at the terminal position-2 is more feasible.

Table 4.7 The optimized energy value and adsorption energy values of CuO and DYD before and after adsorption on three different sites.

Diocetyl phthalate	(before adsorption)	(after adsorption) central	(after adsorption) Terminal 1	(after adsorption) Terminal 2
Opt energy in eV on ADF	-348.7579	-354.5511	-355.7575	-355.3072
Enthalpy (ΔH)(eV)	-364.5438	-370.9291	-372.4121	-371.9793
Entropy (S)(kcal/mol-K)	218.365	228.578	235.953	-233.456
$\Delta G = \Delta H - T\Delta S$ T=298.15(kcal/mol)	-64345.4888	-67344.2831	-69506.6411	-68774.5873
$\Delta E_{adp} = -\text{composite}-(NP+dye)$ (eV)	----	-2.0694	-3.2758	-2.8255

The binding energy of DYD before adsorption was -348.7579, after adsorption it decreased to -355.7575eV, -355.3023eV and -354.7579eV in central, terminal 1 and terminal 2 positions, respectively. When the process of adsorption takes place the Gibbs free energy value also decreases so, before adsorption it was -64345.4888, after adsorption it is decreased to -67344.2831eV, -69506.6411 and -68774.5873eV in central, terminal 1 and terminal 2 positions, respectively which shows it is a spontaneous process. A negative value of interaction energy (ΔG) represented the favored adsorption whereas positive value indicated the theoretically unfavored interaction of adsorbate with adsorbant. The negative values of adsorption energy show it are an exothermic process. So, if we compare the adsorption energy values terminal 1 shows the highest possible attraction of CuO with DYD.

Chapter 5 Discussion:

Water pollution has consistently posed an environmental problem and a global challenge. This is mainly attributed to the rising rate of human activities, including population growth, industrialization, and agricultural practices, which have raised concerns about water quantity, quality, and availability in numerous regions worldwide. Various methods have been developed to address dye waste treatment, such as coagulation-flocculation, biodegradation, electrochemical oxidation, ion exchange, Fenton oxidation, reverse osmosis, ozonation, electrocoagulation, and adsorption. Nevertheless, these approaches are both time and energy-intensive, as well as cost-ineffective in meeting the rigorous standards for water quality. Therefore, to address the challenges posed by water pollution, it is imperative that new technologies arise to ensure the provision of clean and accessible water to various regions across the globe.

Nanotechnology stands out as one of the leading innovative technologies for advancing water purification processes, ranking among the top five. This is attributed to its extensive applications in preventing water pollution, detecting contaminants, monitoring water quality, and remediating pollutants, all while remaining cost-effective. The distinctive characteristics of nanomaterials, including their high surface area, photosensitivity, catalytic and antimicrobial activity, electrochemical, optical, and magnetic properties, as well as tunable pore size and surface chemistry, contribute to their versatile range of applications.

Nanoparticles (NPs) refer to particles with dimensions ranging from 1 to 100 nm, making them highly significant in eliminating pollutants from aqueous environments. These particles are derived from metals and metal oxides, including Titanium dioxide, metal oxide nano-materials,

cupric oxide, and others. In this research we focused on the removal of three waste water components such as Bifenthrin (pesticide), Dioctylphthalate (phthalate) and direct yellow dye (dye).

From the literature review, we have observed that certain metal oxide NPs, such as Titanium oxide (TiO₂) Nanoparticles and zinc oxide nanoparticles, have been used to remove these components from water. However, the limitation with these nanoparticles is that TiO₂ is highly effective but also expensive, while zinc oxide nanoparticles are cost-effective but pose toxicity issues, leading to severe health problems. Considering these factors, our research goal was to identify an adsorbent that is less expensive and capable of removing a maximum number of pollutants and their components from water.

Copper is a naturally occurring element found ubiquitously in the environment, with a concentration of approximately 60 grams per ton in the Earth's crust. The water treatment, textile industries, food preservation, and agricultural practices, among other applications, find copper-based nanoparticles suitable due to their antimicrobial and antifungal properties. Copper oxide nanoparticles (CuO NPs) demonstrate effectiveness in adsorption and exhibit versatility in various applications due to their small size, high surface area, the natural abundance of their starting material, cost-effective production processing, and non-toxic nature.

So, in this research all model geometries of wastewater components: dyes (direct yellow dye), pesticide (bifenthrin) and phthalate (dioctyl phthalate) were initially optimized using GGA-PW91/DZ level of density functional theory method. Frequency calculations were then performed on the optimized geometries for validation. After that we adsorbed copper oxide nanoparticles on three different waste water components such as bifenthrin, dioctyl phthalate, and direct yellow dye to clean the water by using the same level of DFT theory. According to the optimized data CuO

NP shows the strong adsorption towards oxygen and hydrogen side of bifenthrin pesticide which is -0.3767eV . In case of dioctyl phthalate CuO NP shows adsorption from one ester terminal site which is -2.5783eV . In case of Direct yellow dye terminal 1 shows the best possible adsorption in which -3.2758eV . CuO NPs shows best attraction from sulphonic group site of direct yellow dye.

Comparing adsorption between these three components, Bifenthrin, Dioctyl phthalate and Direct yellow dye, direct yellow dye showed the highest attraction towards Copper oxide nanoparticles as it showed the highest negative adsorption energy value which is -3.2758eV .

Chapter 6 Conclusion

In this study, waste water treatment using Copper Oxide (CuO) nanoparticles are investigated using the density functional method GGA-PW91 on Amsterdam Density Functional (ADF) 2019 software. A comprehensive computational investigation spanning electronic, and thermodynamic domains was conducted to examine the adsorption behavior of bifenthrin, direct yellow dye, and dioctyl phthalate on Copper Oxide. Comparative analysis revealed that among these components, direct yellow dye exhibited the highest affinity toward Copper Oxide nanoparticles. This observation is verified by the manifestation of the most negative adsorption energy value (-3.2758 eV) and smaller HOMO-LUMO energy gap, indicating maximal adsorption constant values and enhanced spontaneity in heterogeneous processes. Furthermore, we anticipate the feasibility of conducting a dual-pronged study encompassing both computational simulations and experimental methodologies to further elucidate the complexities of the adsorption process.

6.1 Future Perspectives

Pesticides, phthalates, dyes being used in different areas and released as waste in water, impose deteriorating effect on environment by affecting the aquatic organism, forest, and humans through drinking water. Current research will be helpful for the removal of these dyes pollutants from wastewater by adsorption on the surface of Copper Oxide (CuO) nano-particles. The foremost benefit of the current research in the future will be the treatment of water, and the recycling to be used as molecular sieves effectively. Research include computational methods to be used for the

removal of a large variety of molecular partially insoluble waste in water. At present, the one of the serious challenges encountered over the world is the clean drinking water scarcity which can be achieved using modern heterogeneous adsorption procedures. In upcoming studies, scientists may employ the adsorbent to address newly identified environmental contaminants that have emerged as concerns in modern times. The findings of this research suggest that CuO NPs serve as an efficient adsorbent for effectively reducing various pollutants in the aqueous environment.

References

1. Tiginyanu, I., et al., *Nanostructures of metal oxides*. 2011.
2. Sathiya, S., G. Okram, and J.J.A.M.P. Rajan, *Structural, optical and electrical properties of copper oxide nanoparticles prepared through microwave assistance*. 2017. **2**(6): p. 371-377.
3. Soon, A., et al., *Thermodynamic stability and structure of copper oxide surfaces: A first-principles investigation*. 2007. **75**(12): p. 125420.
4. Baylan, N., et al., *Copper oxide nanoparticles as a novel adsorbent for separation of acrylic acid from aqueous solution: synthesis, characterization, and application*. 2020. **231**: p. 1-15.
5. Rajput, V., et al., *Interaction of copper-based nanoparticles to soil, terrestrial, and aquatic systems: critical review of the state of the science and future perspectives*. 2020: p. 51-96.
6. Ahamed, M., et al., *Synthesis, characterization, and antimicrobial activity of copper oxide nanoparticles*. **2014**: p. 17-17.
7. Elazab Dr, H.A., *The catalytic activity of copper oxide nanoparticles towards carbon monoxide oxidation catalysis: microwave–assisted synthesis approach*. 2018.
8. El-Trass, A., et al., *CuO nanoparticles: synthesis, characterization, optical properties and interaction with amino acids*. 2012. **258**(7): p. 2997-3001.
9. Chen, P.-H., W.-J. Chen, and J.-Y.J.C. Tseng, *Thermal Stability of the Copper and the AZO Layer on Textured Silicon*. 2021. **11**(12): p. 1546.

10. Guzman, M., et al., *Effect of the concentration and the type of dispersant on the synthesis of copper oxide nanoparticles and their potential antimicrobial applications*. 2021. **6**(29): p. 18576-18590.
11. Schedel-Niedrig, T., et al., *Copper (sub) oxide formation: a surface sensitive characterization of model catalysts*. 2000. **2**(10): p. 2407-2417.
12. Ighalo, J.O. and A.G.J.C. Adeniyi, *A comprehensive review of water quality monitoring and assessment in Nigeria*. 2020. **260**: p. 127569.
13. Ighalo, J.O., et al., *CuO nanoparticles (CuO NPs) for water treatment: A review of recent advances*. 2021. **15**: p. 100443.
14. Singh, M.R. and A.J.C.f.B. Gupta, Department of Botany, Nagaland University, *Water pollution-sources, effects and control*. 2016: p. 1-16.
15. Owa, F.J.M.j.o.s.s., *Water pollution: sources, effects, control and management*. 2013. **4**(8): p. 65.
16. Kant, R., *Textile dyeing industry an environmental hazard*. 2011.
17. Solís, M., et al., *Microbial decolouration of azo dyes: a review*. 2012. **47**(12): p. 1723-1748.
18. Gholami-Borujeni, F., et al., *Application of immobilized horseradish peroxidase for removal and detoxification of azo dye from aqueous solution*. 2011. **15**(2): p. 217-222.
19. Rodríguez-Couto, S., J.F. Osma, and J.L.J.E.i.L.S. Toca-Herrera, *Removal of synthetic dyes by an eco-friendly strategy*. 2009. **9**(2): p. 116-123.
20. Joshni, T.C. and K.J.I.J.o.E.S. Subramaniam, *Enzymatic degradation of azo dyes-a review*. 2011. **1**(6): p. 1250-1260.

21. Pan, Y., et al., *Removal of azo dye in an up-flow membrane-less bioelectrochemical system integrated with bio-contact oxidation reactor*. 2017. **326**: p. 454-461.
22. Dos Santos, A.B., F.J. Cervantes, and J.B.J.B.t. Van Lier, *Review paper on current technologies for decolourisation of textile wastewaters: perspectives for anaerobic biotechnology*. 2007. **98**(12): p. 2369-2385.
23. Al-Alwani, M.A., et al., *Application of dyes extracted from *Alternanthera dentata* leaves and *Musa acuminata* bracts as natural sensitizers for dye-sensitized solar cells*. 2018. **192**: p. 487-498.
24. Crini, G.J.B.t., *Non-conventional low-cost adsorbents for dye removal: a review*. 2006. **97**(9): p. 1061-1085.
25. Forgacs, E., T. Cserháti, and G.J.E.i. Oros, *Removal of synthetic dyes from wastewaters: a review*. 2004. **30**(7): p. 953-971.
26. Ge, F., et al., *Efficient removal of cationic dyes from aqueous solution by polymer-modified magnetic nanoparticles*. 2012. **198**: p. 11-17.
27. Raval, N.P., P.U. Shah, and N.K.J.A.W.S. Shah, *Malachite green “a cationic dye” and its removal from aqueous solution by adsorption*. 2017. **7**: p. 3407-3445.
28. Alver, E. and A.Ü.J.C.E.J. Metin, *Anionic dye removal from aqueous solutions using modified zeolite: Adsorption kinetics and isotherm studies*. 2012. **200**: p. 59-67.
29. Attallah, O.A., et al., *Removal of cationic and anionic dyes from aqueous solution with magnetite/pectin and magnetite/silica/pectin hybrid nanocomposites: kinetic, isotherm and mechanism analysis*. 2016. **6**(14): p. 11461-11480.
30. Aziz, E.K., et al., *Adsorptive removal of anionic dye from aqueous solutions using powdered and calcined vegetables wastes as low-cost adsorbent*. 2018. **25**(3): p. 93-102.

31. Khaled, A., et al., *Treatment of artificial textile dye effluent containing Direct Yellow 12 by orange peel carbon*. 2009. **238**(1-3): p. 210-232.
32. Aspland, J.J.T.C. and Colorist, *Disperse dyes and their application to polyester*. 1992. **24**: p. 18-18.
33. Aspland, J.J.T.C. and Colourists, *Vat dyes and their application*. 1992. **24**: p. 22-24.
34. Chen, M., et al., *Removal of azo dyes from water by combined techniques of adsorption, desorption, and electrolysis based on a supramolecular sorbent*. 2013. **52**(6): p. 2403-2411.
35. Fernandes, N.C., et al., *Removal of azo dye using Fenton and Fenton-like processes: Evaluation of process factors by Box–Behnken design and ecotoxicity tests*. 2018. **291**: p. 47-54.
36. Foster, S.L., et al., *Removal of synthetic azo dye using bimetallic nickel-iron nanoparticles*. 2019. **2019**.
37. Saroyan, H., G.Z. Kyzas, and E.A.J.P. Deliyanni, *Effective dye degradation by graphene oxide supported manganese oxide*. 2019. **7**(1): p. 40.
38. Al-Saleh, I.A.J.J.o.e.p., toxicology, o.o.o.o.t.I.S.f.E. Toxicology, and Cancer, *Pesticides: a review article*. 1994. **13**(3): p. 151-161.
39. Kudsk, P. and J.J.W.R. Streibig, *Herbicides—a two-edged sword*. 2003. **43**(2): p. 90-102.
40. Morton, V. and T.J.A.F. Staub, *A short history of fungicides*. 2008. **308**: p. 1-12.
41. Murphy, M.J.J.V.C.S.A.P., *Rodenticides*. 2002. **32**(2): p. 469-484.
42. Bradbury, S.P., J.R.J.R.o.e.c. Coats, and toxicology, *Comparative toxicology of the pyrethroid insecticides*. 1989: p. 133-177.

43. Kamrin, M.A.J.J.o.T. and P.B. Environmental Health, *Phthalate risks, phthalate regulation, and public health: a review*. 2009. **12**(2): p. 157-174.
44. Okaya, Y.J.A.C., *The crystal structure of potassium acid phthalate, KC₆H₄COOH.COO*. 1965. **19**(6): p. 879-882.
45. Thomsen, M., et al., *Solubilities and surface activities of phthalates investigated by surface tension measurements*. 2001. **20**(1): p. 127-132.
46. Godwin, A.J.C.H.A.P.o.P., *Uses of phthalates and other plasticizers*. 2010.
47. Sastry, V. and G.J.J.o.a.P. Rao, *Dioctyl phthalate, and antibacterial compound from the marine brown alga—Sargassum wightii*. 1995. **7**: p. 185-186.
48. Xu, J.-l., et al., *Application of nanometer antimony trioxide modified by dioctyl phthalate in polyvinyl chloride flame retardant materials*. 2021. **23**.
49. Katheresan, V., J. Kansedo, and S.Y.J.J.o.e.c.e. Lau, *Efficiency of various recent wastewater dye removal methods: A review*. 2018. **6**(4): p. 4676-4697.
50. Hethnawi, A., et al., *Polyethylenimine-functionalized pyroxene nanoparticles embedded on Diatomite for adsorptive removal of dye from textile wastewater in a fixed-bed column*. 2017. **320**: p. 389-404.
51. Kannan, N., M.M.J.D. Sundaram, and pigments, *Kinetics and mechanism of removal of methylene blue by adsorption on various carbons—a comparative study*. 2001. **51**(1): p. 25-40.
52. Yagub, M.T., et al., *Dye and its removal from aqueous solution by adsorption: a review*. 2014. **209**: p. 172-184.
53. Salleh, M.A.M., et al., *Cationic and anionic dye adsorption by agricultural solid wastes: a comprehensive review*. 2011. **280**(1-3): p. 1-13.

54. Draper, B., et al., *Reducing liver disease-related deaths in the Asia-Pacific: the important role of decentralised and non-specialist led hepatitis C treatment for cirrhotic patients*. 2022. **20**.
55. Hauser, P., *Advances in treating textile effluent*. 2011: BoD–Books on Demand.
56. De Gisi, S., et al., *Characteristics and adsorption capacities of low-cost sorbents for wastewater treatment: A review*. 2016. **9**: p. 10-40.
57. Moon, W.C.J.I.J.o.I.E., *A review on interesting properties of chicken feather as low-cost adsorbent*. 2019. **11**(2).
58. Costanzo, F., et al., *Physisorption, diffusion, and chemisorption pathways of H₂ molecule on graphene and on (2, 2) carbon nanotube by first principles calculations*. 2012. **8**(4): p. 1288-1294.
59. Zhang, B., et al., *Direct comparison between chemisorption and physisorption: a study of poly (ethylene glycol) by means of single-molecule force spectroscopy*. 2017. **7**(54): p. 33883-33889.
60. Abualnaja, K.M., et al., *Removing of anionic dye from aqueous solutions by adsorption using of multiwalled carbon nanotubes and poly (Acrylonitrile-styrene) impregnated with activated carbon*. 2021. **13**(13): p. 7077.
61. Khalaf, I.H., et al., *Optimization of Congo red dye adsorption from wastewater by a modified commercial zeolite catalyst using response surface modeling approach*. 2021. **83**(6): p. 1369-1383.
62. Sharma, K., et al., *Methylene blue dye adsorption from wastewater using hydroxyapatite/gold nanocomposite: Kinetic and thermodynamics studies*. 2021. **11**(6): p. 1403.

63. El-Harby, N.F., et al., *Adsorption of Congo red dye onto antimicrobial terephthaloyl thiourea cross-linked chitosan hydrogels*. 2017. **76**(10): p. 2719-2732.
64. Razi, M.A.M., M.N.A.M. Hishammudin, and R. Hamdan. *Factor affecting textile dye removal using adsorbent from activated carbon: A review*. in *MATEC Web of Conferences*. 2017. EDP Sciences.
65. Valdes, A., et al., *Solar hydrogen production with semiconductor metal oxides: new directions in experiment and theory*. 2012. **14**(1): p. 49-70.
66. Tejada-Tovar, C., Á. Villabona-Ortíz, and Á.D.J.w. Gonzalez-Delgado, *Adsorption of azo-anionic dyes in a solution using modified coconut (Cocos nucifera) mesocarp: Kinetic and equilibrium study*. 2021. **13**(10): p. 1382.
67. Mondal, N.K. and S.J.A.W.S. Kar, *Potentiality of banana peel for removal of Congo red dye from aqueous solution: isotherm, kinetics and thermodynamics studies*. 2018. **8**: p. 1-12.
68. de Farias Silva, C.E., et al., *Basic-dye adsorption in albedo residue: Effect of pH, contact time, temperature, dye concentration, biomass dosage, rotation and ionic strength*. 2020. **32**(6): p. 351-359.
69. Brito, M.J.P., et al., *Adsorption of the textile dye Dianix® royal blue CC onto carbons obtained from yellow mombin fruit stones and activated with KOH and H₃PO₄: kinetics, adsorption equilibrium and thermodynamic studies*. 2018. **339**: p. 334-343.
70. Gamoudi, S. and E.J.J.o.M.S. Srasra, *Adsorption of organic dyes by HDPy⁺-modified clay: effect of molecular structure on the adsorption*. 2019. **1193**: p. 522-531.
71. Yildirim, A.J.C.E. and Technology, *Removal of the anionic dye reactive orange 16 by chitosan/tripolyphosphate/mushroom*. 2021. **44**(8): p. 1371-1381.

72. Khasri, A., et al., *Adsorption of remazol brilliant violet 5R dye from aqueous solution onto melunak and rubberwood sawdust based activated carbon: interaction mechanism, isotherm, kinetic and thermodynamic properties*. 2021. **216**: p. 401-411.
73. Rápó, E., et al., *Adsorptive removal of cationic and anionic dyes from aqueous solutions by using eggshell household waste as biosorbent*. 2018. **65**(3): p. 709-717.
74. Stjepanović, M., et al., *From waste to biosorbent: Removal of congo red from water by waste wood biomass*. 2021. **13**(3): p. 279.
75. Šljivić-Ivanović, M., I.J.A.i.C. Smičiklas, and D.W. Recycling, *Utilization of C&D waste in radioactive waste treatment—Current knowledge and perspectives*. 2020: p. 475-500.
76. Aljeboree, A.M., A.N. Alshirifi, and A.F.J.A.j.o.c. Alkaim, *Kinetics and equilibrium study for the adsorption of textile dyes on coconut shell activated carbon*. 2017. **10**: p. S3381-S3393.
77. Iqbal, J., et al., *Adsorption of acid yellow dye on flakes of chitosan prepared from fishery wastes*. 2011. **4**(4): p. 389-395.
78. Yeow, P.K., S.W. Wong, and T.J.B.R.A.C. Hadibarata, *Removal of azo and anthraquinone dye by plant biomass as adsorbent—a review*. 2021. **11**: p. 8218-8232.
79. Badawy, A.A., et al., *Enhancing the textile dye removal from aqueous solution using cobalt ferrite nanoparticles prepared in presence of fulvic acid*. 2020. **30**: p. 1798-1813.
80. Abdel-Aziz, M.H., et al., *DFT and experimental study on adsorption of dyes on activated carbon prepared from apple leaves*. 2021. **31**: p. 863-878.
81. Revathi, G., S. Ramalingam, and P.J.C.S.T. Subramaniam, *Assessment of the adsorption kinetics and equilibrium for the potential removal of direct yellow–12 dye using *Jatropha curcus L.* activated carbon*. 2014. **3**: p. 93-106.

82. Wang, L.-G. and G.-B.J.D. Yan, *Adsorptive removal of direct yellow 161 dye from aqueous solution using bamboo charcoals activated with different chemicals*. 2011. **274**(1-3): p. 81-90.
83. Wawrzkievicz, M., et al., *Adsorptive removal of CI Direct Yellow 142 from textile baths using nanosized silica-titanium oxide*. 2019. **134**: p. 1-10.
84. Alabbad, E.A.J.A.J.O.C., *Effect of Direct yellow 50 removal from an aqueous solution using nano bentonite; adsorption isotherm, kinetic analysis and also thermodynamic behavior*. 2023. **16**(2).
85. Ghani, S.B.A., *Reduction of Ethion and Bifenthrin Residues in Palm Dates Using Ozonated Water and Metal Ions*.
86. Zhang, M., et al., *Magnetic adsorbent based on mesoporous silica nanoparticles for magnetic solid phase extraction of pyrethroid pesticides in water samples*. 2019. **1598**: p. 20-29.
87. Bakka, A., et al., *Removal of bifenthrin pesticide from aqueous solutions by treated patellidae shells using a new fixed bed column filtration technique*. 2020. **143**: p. 55-65.
88. Carmignani, G. and J.J.A. Bennett, *Filter media for the removal of phthalate esters in water of closed aquaculture systems*. 1976. **8**(3): p. 291-294.
89. Vannucchi, F., et al., *Populus alba dioctyl phthalate uptake from contaminated water*. 2019. **26**: p. 25564-25572.
90. Hosny, N.M., I. Gomaa, and M.G.J.A.S.S.A. Elmahgary, *Adsorption of polluted dyes from water by transition metal oxides: A review*. 2023. **15**: p. 100395.
91. El Maguana, Y., et al., *Activated carbon for dyes removal: modeling and understanding the adsorption process*. 2020. **2020**: p. 1-9.

92. Amalina, F., et al., *Dyes removal from textile wastewater by agricultural waste as an absorbent—a review*. 2022: p. 100051.
93. Jeirani, Z., C.H. Niu, and J.J.R.i.C.E. Soltan, *Adsorption of emerging pollutants on activated carbon*. 2017. **33**(5): p. 491-522.
94. Naseem, T., T.J.E.C. Durrani, and Ecotoxicology, *The role of some important metal oxide nanoparticles for wastewater and antibacterial applications: A review*. 2021. **3**: p. 59-75.
95. Li, W., et al., *Highly efficient iron nanocatalyst stabilized by double-walled carbon nanotubes and mixed metal oxides for degradation of cationic and anionic dyes by a Fenton-like process*. 2014. **53**(47): p. 18095-18103.
96. Falcaro, P., et al., *Application of metal and metal oxide nanoparticles@ MOFs*. 2016. **307**: p. 237-254.
97. Chavali, M.S. and M.P.J.S.a.s. Nikolova, *Metal oxide nanoparticles and their applications in nanotechnology*. 2019. **1**(6): p. 607.
98. Liu, W.-T.J.J.o.b. and bioengineering, *Nanoparticles and their biological and environmental applications*. 2006. **102**(1): p. 1-7.
99. Imamura, K., et al., *Stoichiometric production of aminobenzenes and ketones by photocatalytic reduction of nitrobenzenes in secondary alcoholic suspension of titanium (IV) oxide under metal-free conditions*. 2013. **134**: p. 193-197.
100. Guesh, K., et al., *Enhanced photocatalytic activity of TiO₂ supported on zeolites tested in real wastewaters from the textile industry of Ethiopia*. 2016. **225**: p. 88-97.
101. Bankmann, M., et al., *Forming of high surface area TiO₂ to catalyst supports*. 1992. **14**(2): p. 225-242.

102. Mironyuk, I., et al., *Highly efficient adsorption of strontium ions by carbonated mesoporous TiO₂*. 2019. **285**: p. 742-753.
103. Fazal, T., et al., *Integrating adsorption and photocatalysis: A cost effective strategy for textile wastewater treatment using hybrid biochar-TiO₂ composite*. 2020. **390**: p. 121623.
104. Binaeian, E., S.B. Zadvarzi, and D.J.I.j.o.b.m. Yuan, *Anionic dye uptake via composite using chitosan-polyacrylamide hydrogel as matrix containing TiO₂ nanoparticles; comprehensive adsorption studies*. 2020. **162**: p. 150-162.
105. Kariim, I., et al., *Development of MWCNTs/TiO₂ nanoadsorbent for simultaneous removal of phenol and cyanide from refinery wastewater*. 2020. **10**: p. e00593.
106. Elbarbary, A.M., et al., *Radiation synthesis and characterization of poly (vinyl alcohol)/acrylamide/TiO₂/SiO₂ nanocomposite for removal of metal ion and dye from wastewater*. 2021. **31**(10): p. 4103-4125.
107. Awwad, A., M. Amer, and M.J.C.I. Al-aqarbeh, *TiO₂-kaolinite nanocomposite prepared from the Jordanian Kaolin clay: Adsorption and thermodynamics of Pb (II) and Cd (II) ions in aqueous solution*. 2020.
108. Jena, K.K., et al., *Advanced TiO₂-SiO₂-Sulfur (Ti-Si-S) nanohybrid materials: potential adsorbent for the remediation of contaminated wastewater*. 2019. **11**(33): p. 30247-30258.
109. Abdulhameed, A.S., A.H. Jawad, and A.-T.J.B.t. Mohammad, *Synthesis of chitosan-ethylene glycol diglycidyl ether/TiO₂ nanoparticles for adsorption of reactive orange 16 dye using a response surface methodology approach*. 2019. **293**: p. 122071.
110. Herrera-Barros, A., et al., *Nickel adsorption from aqueous solution using lemon peel biomass chemically modified with TiO₂ nanoparticles*. 2020. **17**: p. 100299.

111. Sharma, M., et al., *Adsorption of heavy metal ions by mesoporous ZnO and TiO₂@ ZnO monoliths: adsorption and kinetic studies*. 2019. **145**: p. 105-112.
112. Chang, L., et al., *Magnetic core-shell MnFe₂O₄@ TiO₂ nanoparticles decorated on reduced graphene oxide as a novel adsorbent for the removal of ciprofloxacin and Cu (II) from water*. 2021. **541**: p. 148400.
113. Zhou, R., et al., *Mild-method synthesized GO-TiO₂ retains oxygen-containing functional groups as an effective adsorbent*. 2021. **301**: p. 122290.
114. Heinonen, S., et al., *Investigation of long-term chemical stability of structured ZnO films in aqueous solutions of varying conditions*. 2017. **638**: p. 410-419.
115. Sruthi, S., J. Ashtami, and P.J.M.t.c. Mohanan, *Biomedical application and hidden toxicity of Zinc oxide nanoparticles*. 2018. **10**: p. 175-186.
116. Primo, J.d.O., et al., *Synthesis of zinc oxide nanoparticles by ecofriendly routes: adsorbent for copper removal from wastewater*. 2020. **8**: p. 571790.
117. Gu, M., et al., *The selective heavy metal ions adsorption of zinc oxide nanoparticles from dental wastewater*. 2020. **534**: p. 110750.
118. Muinde, V.M., et al., *Adsorption of malachite green dye from aqueous solutions using mesoporous chitosan–zinc oxide composite material*. 2020. **2**: p. 115-125.
119. Debnath, P., N.K.J.E.n. Mondal, monitoring, and management, *Effective removal of congo red dye from aqueous solution using biosynthesized zinc oxide nanoparticles*. 2020. **14**: p. 100320.
120. Mittal, H., et al., *In-situ synthesis of ZnO nanoparticles using gum arabic based hydrogels as a self-template for effective malachite green dye adsorption*. 2020. **28**: p. 1637-1653.

121. Rathi, B.S., P.S. Kumar, and D.-V.N.J.S.o.T.T.E. Vo, *Critical review on hazardous pollutants in water environment: Occurrence, monitoring, fate, removal technologies and risk assessment*. 2021. **797**: p. 149134.
122. Hartree, D.R. *The wave mechanics of an atom with a non-coulomb central field. Part II. Some results and discussion*. in *Mathematical Proceedings of the Cambridge Philosophical Society*. 1928. Cambridge University Press.
123. Thomas, L.J.Z.P., *Pmt. Cambridge Philos. Sot., 23 (1926) 542. E. Fermi*. 1928. **48**: p. 73.
124. Thomas, L.t. and K.J.T.J.o.C.P. Umeda, *Atomic scattering factors calculated from the TFD atomic model*. 1957. **26(2)**: p. 293-303.